SOURCES OF THERMALLY GENERATED VACANCIES IN SINGLE-CRYSTAL AND POLYCRYSTALLINE GOLD

BY

DAVID NATHANIEL SEIDMAN
B.Met.E., New York University, 1960
M.S., New York University, 1962

THESIS

Submitted in partial fulfillment of the requirements
for the degree of Doctor of Philosophy in Metallurgical Engineering
in the Graduate College of the
University of Illinois, 1965

Urbana, Illinois

UNIVERSITY OF ILLINOIS

THE GRADUATE COLLEGE

February, 1965

I HEREBY RECOMMEND THAT THE THESIS PREPARED UNDER MY SUPERVISION BY DAVID NATHANIEL SEIDMAN

ENTITLED SOURCES OF THERMALLY GENERATED VACANCIES IN SINGLE-CRYSTAL AND POLYCRYSTALLINE GOLD

BE ACCEPTED IN PARTIAL FULFILLMENT OF THE REQUIREMENTS FOR THE DEGREE OF DOCTOR OF PHILOSOPHY

R W Balluffi
In Charge of Thesis

T. A. Read
Head of Department

Recommendation concurred in†

Marvin Metzger
R W Balluffi
C M Wayman
A. V. Granato
David Lazarus

Committee on Final Examination†

† Required for doctor's degree but not for master's.

D517

ACKNOWLEDGEMENTS

The author would like to thank his thesis advisor, Professor Robert W. Balluffi, for his advice, encouragement and contagious enthusiasm for performing experiments on point defects. He would also like to thank Professor J. S. Koehler and Dr. C. A. Lund for the details of the electrical pulsing circuit and for the loan of equipment. Thanks are also due to Dr. Piers B. Bowden for interesting discussions and a very pleasant friendship during the course of the investigation. In addition he would like to thank Mr. Cary Conley for assistance with the experimental work and Mr. David Hutchinson for programming.

He also wishes to thank the Atomic Energy Commission for their generous support of the research.

TABLE OF CONTENTS

I. INTRODUCTION

Sources of vacancies play an important role in phenomena such as sintering, the Kirkendall effect, high temperature creep, polygonization and many other diffusion controlled processes. In spite of their importance very little is known about the fundamental properties of vacancy sources. For example, it is not known if a vacancy can form with the same ease on a surface, a grain boundary, a sub-boundary and a dislocation. Also, the energy to form a jog on a dislocation, and the rate at which the dislocation climbs are at best poorly understood. Of all the potential vacancy sources the dislocation is the one most studied and least understood.

The electrical pulsing work of Jackson (1960), Lund (1964) and Koehler (1960, 1964) pioneered the study of vacancy generation at high temperatures, when a lattice is subjected to a sudden and large subsaturation of vacancies. Their experiments indicated that vacancies are being produced at dislocations, but the work is hampered by a poor knowledge of the specimen structure (e.g. grain size, subgrain size and dislocation density). Thus their interpretation and conclusions regarding the operative vacancy sources are uncertain. The specimen structure is particularly important if one wishes to observe only the high temperature climb (T/T_m greater than 0.5)* of dislocations. For example Barnes (1960) has shown

---

*T and T_m are the temperature and melting temperature respectively (in units of ^{o}K).

that the free surfaces and grain boundaries in copper are excellent sources of thermally generated vacancies, though he found no definitive evidence for dislocation climb.

In view of the existing situation an investigation was undertaken to study vacancy generation in specimens with a controlled structure. A new technique is developed for thermally pulsing thick single crystals and distinguishing internally produced vacancies from vacancies generated at the free surfaces. In addition the Lund-Koehler (1964) electrical pulsing technique is used and extended to study generation (formation) kinetics in polycrystalline specimens whose dislocation density, subgrain size and grain size are measured. Analyses are performed, based on the present experimental data, to account for possible dislocation shortcircuiting and distinguishing between vacancy diffusion limited climb and vacancy production limited dislocation climb.

Gold is the logical choice for the present study since: (1) the high temperature monovacancy diffusion coefficient and equilibrium concentration are known (Simmons and Balluffi, 1962), (2) the specimens are readily thinned for observation by transmission electron microscopy, (3) previous kinetic studies are available for a comparison with the data obtained, (4) specimens are not contaminated by heating and cooling in air.

II. EXPERIMENTAL PROCEDURE

A. Specimen Procedure

1. Polycrystalline Foils

All of the polycrystalline specimens used were prepared from COMINCO Grade 69 gold of nominal purity 99.9999 weight per cent gold. Detectable impurities are 0.1 ppm Cu, 0.1 ppm Mg and 0.1 ppm Ag.

The specimens were received in the form of a ribbon 0.0178 cm to 0.0191 cm thick, 0.089 cm wide and 18 cm long. The rectangular cross-section permits the specimens to be readily electro-thinned for examination by transmission electron microscopy, after the electrical resistivity measurements are completed. In this manner the microscopic data may be correlated with the detailed specimen microstructure.

The specimen geometry and the copper frame used to hold the specimen are similar to those employed by Ytterhus (1964). The specimen's central gauge length is 7.5 cm and there is also an expansion loop at either end of this central section. The loops help to maintain a uniform temperature distribution and allow unrestrained expansion. The foil is mounted on the copper frame so that the entire gauge length enters the water simultaneously edge-on.

The as-received foils are cleaned with deionized water, acetone, methanol and absolute alcohol. They are then annealed for 15 min. at 100^{o}C. Next they are bent to shape

and mounted on the copper quenching frame. At this point, two 0.00508 cm diam gold potential lead wires are tied to the specimen gauge length at a spacing of 4 to 5 cm. The specimen is then cleaned in the following solutions:

a. 1/2 concentrated HNO_3 - 1/2 H_2O

b. deionized H_2O

c. methonal

After drying, the specimens are annealed for a minimum of 2 hours in air, at temperatures in the range 900-1000°C. The air anneal serves to purify the gold (Ytterhus and Balluffi, 1965), promote grain growth, reduce the dislocation density and sinter on the potential leads. The specimen is then cooled to room temperature at a rate of about 700°C hr^{-1} with a 20 min arrest at 400°C. The slow cooling rate prevents vacancies from being air-quenched into the specimen. (For a detailed discussion of the importance of the pre-quench annealing procedure see the thesis of J. Bass (1964)).

Resistivity ratios, $\mathcal{R}$ ($\mathcal{R} = R_{25°C}/R_{4.2°K}$), between 4000 and 5500 are consistently obtained with the above cleaning and annealing operations. Between every pulse and down-quench the above processing treatments are repeated.

2. Single Crystals

Single crystals of gold are grown from the liquid in the form of a cube, 1.27 cm on a side, by a modified Bridgman technique. The crystals are grown in National Carbon spectroscopically pure graphite molds in an atmosphere of high purity

nitrogen. The starting material is 99.999 weight percent pure gold, purchased from the American Smelting and Refining Corporation, with an $\mathcal{R}$ of about 1200.

After the crystals are grown slabs are cut, with the dimensions 0.318 cm x 0.114 cm x 1.2 cm, from the initial single crystals. The cutting operation is performed on a modified SPARCATRON spark cutter using the slowest cutting rate obtainable on this machine. To bring the specimens to the final desired size and to remove any deformation caused by the spark cutter the crystals are chemically polished. A 1:1 mixture of concentrated HNO_3 and HCl acid, which is brought to a very gentle boil, is used for the polishing. A boiling rate of several bubbles min^{-1} is found to give an excellent polish and a uniform removal rate of material. The polishing is stopped when the crystal reaches a thickness of 0.0508 cm.

The last step in the procedure is to anneal the crystals to reduce the free dislocation density and cause subgrain growth. The gold slabs are then placed on a block of spectroscopically pure graphite and furnace annealed at 1025°C for three days. The furnace is continually flushed with high purity nitrogen except for the last hour of the anneal which is performed in an oxygen atmosphere in order to purify the crystals (Ytterhus, 1964).

Examination of a control specimen, by transmission electron microscopy, indicates that the above procedure produces a single crystal free of deformation and fine scale substructure. Prior to the final anneal, back-reflection

Laue X-ray patterns and Schulz X-ray patterns (Schulz, 1954) are taken to check for deformation and to determine the sub-grain size. The single crystals prepared as described above are used in all the gas pulsing experiments.

B. Pulsing Techniques

1. Electrical Pulsing Method

The polycrystalline foils are pulsed from an initial temperature ($\overline{T}_i$) to a final temperature ($\overline{T}_f$) in 10 to 20 msec and held at $\overline{T}_f$ for times ranging from 20 msec to 1.5 sec and then downquenched. The circuit used to accomplish the pulsing and quenching is almost identical to the one employed by Lund (1964). The details of operation are best explained with the aid of Fig. 1.

The three essential portions of the circuit which must function in rapid succession if a specimen is to be pulsed and downquenched are:

(i) The Wheatstone Bridge and fuse circuit,

(ii) Thryratron circuit and associated relay,

(iii) Attenuator circuit and oscilloscope.

In section (i) the specimen (S) comprises one arm of a Wheatstone Bridge and is heated with a 6 v battery. The temperature of the specimen is determined from its resistance, which is measured by the ammeter-voltmeter method. The 0.0254 cm copper fuse is left out of the circuit until all balancing operations are completed. With switch A in position I the specimen is brought to the pre-pulse temperature ($\overline{T}_i$) by ad-

justing the resistors RI. The temperature $\overline{T}_i$ is usually 200°C to 250°C below the final temperature ($\overline{T}_f$). Switch A is then placed in position II and the resistors RII adjusted to bring the specimen to its final temperature ($\overline{T}_f$). While the specimen is at $\overline{T}_f$ the 0-5K potentiometer is adjusted until the trace on the oscilloscope screen is balanced at zero deflection. Next, switch A is returned to position I and a copper fuse is placed in its holder. To pulse the specimen switch A is returned rapidly to position II. This action places 30 v across the specimen and fuse and results in a large initial current through the specimen, which brings the foil to temperature ($\overline{T}_f$) in 10 to 20 msec. The resistance of the fuse is such that it burns out by the time the specimen has reached $\overline{T}_f$ and thus simply serves to bring the specimen to temperature. Once the specimen is at temperature the 6 v battery supplies the necessary heating current. The entire process is recorded on an oscillogram, so that a temperature-time history is available for every pulse. A typical oscillogram is shown in Fig. 2A.

Section (iii) contains the thyratron circuit which operates the dropping relay. The purpose of the relay is to release the copper quenching frame into the bath. After the bridge is balanced at $\overline{T}_f$ and switch A returned to position I then switch B is closed. This charges C_2 and thus places the plate of the thyratron at +390 v DC. Next the 10K potentiometer and the 2-357μf capacitor are adjusted in the grid circuit. The RC value chosen determines the rate at which

the -6v on the grid leaks off and therefore determines the time before the tube fires and the relay opens. The range of RC is large enough to allow pulses of 0.020 to 3 sec.

The third section contains the oscilloscope and attenuator relay. The scope is placed in the position normally occupied by a galvanometer in a Wheatstone Bridge. The attenuator circuit is designed so that the scope only sees a small portion of the actual voltage when the bridge is severely out of balance, i.e. when switch A is in position I. A Tektronix 545A is employed to record the trace and is fired internally by the rising signal. The 5 mv cm^{-1} scale on a Type D pre-amplifier is employed in all the experiments and gives a sensitivity of $7.5^{\circ}C\ cm^{-1}$.

After a specimen is pulsed and downquenched it is cooled by lowering it, within 30 sec, into a vertical test tube almost completely immersed in liquid nitrogen.

2. Gas Jet Pulsing of Single Crystal

The apparatus used to pulse and quench the single crystals is drawn schematically in Fig. 3. The single crystal is pulsed from room temperature to temperatures in the range $875^{\circ}C$-$920^{\circ}C$ by a stream of heated compressed air. By passing compressed air through 4.88 m of a resistance heated inconel tube it is brought to the required quench temperature ($\overline{T}_f$).

A single crystal is quickly inserted into the hot air beam, brought to temperature and then pivoted out of the beam and downquenched into a brine solution. The thermal history

of the specimen is measured by using a dummy specimen with a chromel-alumel thermocouple imbedded in it. The emf produced by the thermocouple is fed into either a potentiometer or a Tektronix 545A oscilloscope. An oscillogram of a thermal pulse is seen in Fig. 2B. After downquenching the single crystals are annealed for several hours at 60°C to precipitate the quenched-in vacancies as stacking fault tetrahedra.

The upquenching portion of the thermal pulse is exporential and is described by the equation

$$T(t) = T_o + \Delta T\ (1-e^{-\alpha t}), \qquad 1.$$

where T_o is room temperature, T is the temperature interval over which the single crystal is pulsed, t the time in sec and α the rate constant. A typical value of α for a 0.0508 cm thick crystal is 5.5 sec^{-1}. The downquenching rate is 1.0 to $1.5 \cdot 10^4$ °K sec^{-1}.

C. Measurement of the Specimen Resistance

The helium temperature (4.2°K) resistance is measured by standard potentiometric technique. A Honeywell No. 2768 6-dial potentiometer is used to determine the potential drop across the specimen and a Leeds and Northrup K-3 potentiometer measures the potential drop across a 0.01Ω standard resistor in order to ascertain the current through the specimen. Three Willard No DH-5-1 2v batteries connected in series are used to supply a measuring current of three amp. With the above arrangement a precision of $\pm 10^{-12}\Omega$-cm is attained.

Before inserting the specimen into liquid helium, for

a measurement, it is pre-chilled at 78°K. This is accomplished by inserting the quenching frame into a vertical test tube almost completely immersed in liquid nitrogen. Use of this chilling procedure is helpful in reducing the deformation associated with submerging a warm specimen directly into liquid helium.

The room temperature resistance is measured with the same potentiometric set-up as at helium temperature. During the measurement the specimen is immersed in a temperature monitored bath of water, and a measuring current of 0.200 amp is employed. The fractional error ($\Delta R/R25^{\circ}C$) in room temperature resistance is $1.08 \cdot 10^{-3}$, which is equivalent to an error of 0.312°C. This error in room temperature resistance causes an error of 1.38°C in going to 653°C and an error of 1.74°C upon reaching 878°C. An additional uncertainty in temperature is caused by the measurement of the specimen resistance at temperature, by the ammeter-volt meter method. For the high temperature resistance the fractional error is $2.5 \cdot 10^{-3}$ with the 0.25% accuracy meters used. This brings the total error in temperature measurement to 3.65°C at 653°C and 4.5°C at 877°C.

The resistance ratio $R(T)/R_{25^{\circ}C}$ is used to convert resistance readings into °C. This ratio is obtained from the date of Meechan and Eggleston (1954).

D. Specimen Structure

1. Dislocation Density

The dislocation density of the polycrystalline foils is

measured by transmission electron microscopy. All observations are performed using a Siemens Elmiskop I operating at 100 KV at a standard magnification of 15,000 x.

The density (total line length cm^{-3}) is determined from the relationship, $N_d = 2\ N/A$, where N is the number of dislocations making intersections with both surfaces in an area A (Smith and Guttman, 1953, Frank, 1957, Ham and Sharpe, 1961). This method is the proper one to use as it eliminates an important systematic error present in the techniques described by Bailey and Hirsch (1960) and Ham (1961). The methods of the latter authors depend on the assumption that the dislocation segments are randomly oriented with respect to the surface of the thin films. This is generally not the case, since dislocation orientations normal to the film surface are favored (Ham and Sharpe, 1961).

There are several other systematic errors which also affect the measured dislocation density. They are:

1) A loss of dislocations from the film during thinning.
2) A gain due to handling procedure.
3) A reduction in the dislocation density as a result of dislocations being out of contrast.

The following precautions are taken in an effort to eliminate the above mentioned systematic errors.

1) The densities reported are for micrographs taken in the thickest sections of the specimens, far from the edge of the foil.

2) Three-quarters of every gauge length is sampled, and at least several mm of foil are thinned away before a new specimen is cut. Any specimen which is found to have very long dislocations parallel to the foil surface is discarded. This type of dislocation has been shown to be due to handling (Basinski, 1964).

3) The specimen yielding any given field of view is tilted until the maximum number of dislocations appear.

As a control on the handling and thinning procedure, two well annealed gold foils were neutron irradiated with 10^{17} fast neutrons cm^{-2}. A special jig obviated any need to touch the specimens until the electrothinning procedure started. The purpose of the irradiation is to pin the existing dislocations and hence make their escape from the thinned film difficult. The irradiation also serves to raise the yield stress of the specimens, thus making any deformation due to handling more difficult. The irradiated specimens had an average dislocation density of $(3.17 \pm 2.36)\ 10^{7}$ cm cm^{-3} which is within the average deviation of the measured densities of the specimens used in the actual experiments.

The densities reported here are for free dislocations, as opposed to dislocations grouped in well defined sub-boundaries. In all, over 1100 plates were used in determining the reported values.

2. Grain Size

The average cross-sectional area, $\bar{A}$, of contiguous cells

of the same type is A/N (Smith and Guttman, 1953). The microstructure is recorded by standard metallographic techniques and $\bar{A}$ determined for all the specimens. If a recrystallization twin appears in a grain then that grain is counted as two grains. This procedure is adopted because Barnes (1960) has shown that incoherent portions of the twin boundary can act as channels for vacancies.

For the diffusion calculations the grains are assumed to be approximated by cylinders with their radius (a) given by $(\bar{A}/\pi)^{1/2}$.

3. Subgrain Size

The subgrain size is determined by the standard Schulz and back reflection Laue X-ray techniques.

All of the single crystals and a few of the polycrystalline specimens are examined by the back reflection Laue technique. In this method the resolving power is limited by the angular divergence α ($\alpha = d/L$),* of the incident beam. For the single crystals d is 0.0762 cm, while for the polycrystalline specimens d is 0.0254 cm and L is 5.7 cm for both. Therefore two subgrains can be resolved if α (their angular tilt) is greater than $8.92 \cdot 10^{-3}$ rad or 26.81 rad for the 0.0254 and 0.0762 cm pinholes respectively. The average subgrain area, $\bar{A}$, is A/N where A is the irradiated area and N is the number of subspots within a main Laue spot. It is then assumed that a

---

*d is the diam. of the collimator pinhole and L the half length of the collimator.

satisfactory geometrical model for a subgrain is a sphere and thus the average radius is given by $(\bar{A}/\pi)^{1/2}$.

Schulz patterns are taken of all the single and polycrystalline specimens. White radiation from a fine focus X-ray source (a Hilger microfocus unit with a 40μ focal spot) impinges on the specimen at an angle of incidence of 25°. The pattern is recorded on Ilford G X-ray film which is placed parallel to the specimen. Since a Schulz pattern is a magnified Laue spot the average cross-sectional area is readily obtained and this is then converted to an average radius as is previously discussed.

E. Test for Deformation in the Electrically Pulsed Specimens

The passage of a current through a conductor results in the production of internal stresses because of the interaction of the magnetic fields and the current (see Appendix G). A large current can cause a specimen to pinch itself off and thus the origin of the name "Pinch Effect" (Northrup, 1907).

This phenomenon is relevant to the present work because a large current is used to bring the specimen rapidly to temperature. If the specimen is pinched plastically then dislocation motion and generation take place during the upquench. The act of pulsing can therefore cause a change in the initial static dislocation density in addition to producing a certain concentration of defects due to non-conservative motion of dislocations. In the early work of Jackson a capacitor was discharged across the specimen in order to bring

it rapidly to temperature. The specimen became visibly twisted after several pulses (J. S. Koehler, 1964) and it is obvious that the specimen underwent deformation.

To detect the possible deformation caused by the electrical fuse pulsing technique two control specimens are employed. The first specimen is used to test the effect of handling. It is passed through the following cycle:

1. Chilled to 78°K
2. Inserted in liquid He (4.2°K)
3. Resistance measured at 4.2°K
4. Warmed up to room temperature
5. Start cycle again at 1.

This sequence is repeated 25 times.

The second specimen is subjected to the following treatment:

1. Pulsed several times from 436°C to 653°C
2. Temperature reduced from 653°C to 436°C manually by throwing switch A to position I
3. Annealed 15 min at 436°C
4. Cooled to room temperature at a rate of 20°C min^{-1}.
5. Identical to steps 1-4 for first control.
6. Cleaned (see Sec. A.1)
7. Cycle repeated

This cycle is repeated 17 times.

III. EXPERIMENTAL RESULTS

A. Pulsing of Gold Single Crystals in the Temperature Range 875°C to 920°C

When considering vacancy generation kinetics a very crucial question must be answered in an unequivocal manner. The question is simply whether the predominant sources are internal or external. In a single crystal one would like to know if the dislocations (both freely distributed and grouped in sub-boundaries) can supply the equilibrium concentration of vacancies or does the lattice have to wait for the vacancies to diffuse in from the surfaces in order to reach equilibrium.

The above question is answered by the thermal pulsing experiment. After the pulse, downquench and annealing (see Sec. II B2) treatment each specimen is thinned so that the central plane of the crystal is examined in the transmission electron microscopy studies. In all of the pulsed specimens listed in Table I uniform dense distributions of tetrahedra are always found in the electron microscope observations. The implications of this observation is that vacancies are generated during the pulse, in a high enough concentration to nucleate tetrahedra. Several control specimens are also equilibrated in this temperature range, downquenched, annealed and examined by transmission electron microscopy. The control specimens are similar in structure to the pulsed specimens and contain approximately the same density of tetrahedra. In addition, the densities in the pulsed specimens are similar

over the range of a factor of 2-1/2 in the equivalent time at temperature (teq.). As a further check the density and mean edge length of specimen 2 listed in Table I is measured. The density is $6 \cdot 10^{15} cm^{-3}$, and the mean edge length is 64 A. The apparent vacancy concentration is therefore $2.48 \cdot 10^{-5}$ on the assumption that the observed precipitates are simple stacking fault tetrahedra. This result is in excellent quantitative agreement with the recent measurements of Siegel (1965) who examined vacancy precipitation in quenched gold which was fully equilibrated at the quench temperature.* The similarity of these results indicates that the vacancy equilibrium concentration in this specimen is attained before the downquench.

The above experimental result may be placed on a quantitative basis by solving the diffusion equation for the maximum possible inward flux of vacancies from the three possible sources in well annealed single crystals, which are; (1) Exterior surfaces; (2) Sub-boundary walls; (3) Free dislocations. A temperature dependent monovacancy diffusion coefficient and time dependent equilibrium boundary conditions are employed. The latter boundary condition maximizes the source effectiveness and therefore is an upper limit to the mean vacancy concentration available from a given source. The results of this calculation** for some typical source sizes are indicated

---

*We note this concentration is less than would be expected from equilibrium vacancy concentration measurements (Simmons and Balluffi, 1962). However Siegel (1965) has concluded that the tetrahedral defects in quenched gold are not always simple stacking fault tetrahedra.

**The details of the calculation are given in Appendix A.

TABLE I

SPECIMEN STRUCTURE AND THERMAL HISTORY OF PULSED SINGLE CRYSTALS

Spec.No.	T(^{o}C)	Δt^{t}(sec)	teq.* (sec)	$\frac{C(x=0)}{C_o}$**	Average subgrain radius from Laue spots(μ)
1	916.5	4	--	--	--
2	918.5	1.6	1.4	10^{-4}	--
3	876	2.8	1.66	10^{-4}	245
4	906	1.75	1.53	10^{-4}	245
5	892	2	1.78	10^{-4}	301
6	871	1.85	1.00	10^{-4}	212
7	919	2.6	2.5	10^{-4}	190
8	889	2.2	1.98	10^{-4}	173

^{t} Δt is the total time to go from temperature to the time the downquenching starts.

*teq. is the equivalent time at temperature (T^{o}C)

**$C(x=0)/C_o$ is the fractional vacancy concentration in the central plane of the specimen calculated using Carslaw and Jaeger's (1959) tabulations for our teq.

graphically in Fig. 4. The computed curves for the slab are used to determine t_{eq}. (See Table I), by comparing these curves with their respective isothermal solutions. For all the equivalent times listed in Table I, the value of $D_{1v}t_{eq}/l^2$ is less than 0.03, where D_{1v} is the monovacancy diffusion coefficient and l the half thickness of the slab. For $D_{1v}t_{eq}/l^2$ equal to 0.03 the vacancy concentration profile is such that C (X)*is less than $10^{-3}C_o$ for X/l between zero and 0.3 (Carslaw and Jaeger, 1959). This result indicates that the vacancy concentrations stored in the observed tetrahedra in the central plane of the single crystal cannot be the result of vacancies diffusing from the free surface, but instead are the consequence of internal vacancy production. Therefore we conclude that dislocations readily climb and are the sources** of the observed thermally generated vacancies.

B. Pulsing of Polycrystalline Specimens

1. Vacancy Generation Kinetics at 653°C

The data in Fig. 4 represent the vacancy generation

---

*C (X) is the vacancy concentration as a function of position in the single crystal, where X=0 is the central plane and X=1 is the plane of the outside surface.

**By sources we mean the ultimate sources, i.e. the places where the vacancies are generated. In Appendix C it is definitively shown that the dislocations are not merely acting as vacancy pipes with the surface serving as the ultimate source. Therefore we re-emphasize that the term source and place of generation are synonymous.

kinetics at 653.3°C ($\bar{T}_f$). The mean fractional vacancy fillup in the lattice after t sec at $\bar{T}_f$ is denoted by,

$$f(t) = \frac{\bar{C}(t) - C_i}{C_o - C_i}, \qquad 2.$$

where C_i is the initial concentration at t = 0, C_o is the equilibrium concentration at $\bar{T}_f$ and $\bar{C}(t)$ is the concentration after t sec at 653.3°C ($\bar{T}_f$). In this particular case C_i is the concentration for $\bar{T}_i$ equal to 436.2°C. Experimentally the vacancy concentrations are replaced by the quantities $\Delta R/R_{25°C}$, so that Eq. 2 becomes,

$$f(t) = \frac{\Delta R(t)/_{R_{25°C}} - \Delta R_i/_{R_{25°C}}}{\Delta R_o/R_{25°C} - \Delta R_i/R_{25°C}} \qquad 3.$$

The values of $\Delta R_o/R_{25°C}$ and $\Delta R_i/R_{25°C}$ are taken from the recent precise determinations of Bass (1964), after the initial and final temperatures are measured for each pulse. The quantity $\Delta R(t)$ is measured at 4.2°K, and the time (t) is read off the oscillogram. The error bar associated with each point reflects the uncertainty in vacancy concentration due to the uncertainty in temperature.

To correlate the macroscopic resistivity data with actual specimen structure, the grain size, the subgrain size and dislocation density are measured for the resistivity specimens. All of these parameters are listed in Table II for the electrically pulsed specimens, and composite histograms of the

TABLE II

STRUCTURE OF POLYCRYSTALLINE ELECTRICALLY PULSED SPECIMENS

Specimen Number	($cm.cm^{-3}$) $.10^{-7}$ Nd.	average subgrain radius from Schulz patterns(μ)	average grain radius(μ) (untwinned)	average grain radius(μ) (twinned)
21	7.9±6.1	111.4	138.4	130
24	8.0±4.85	84.1	169.6	141.2
25	6.89±3.8	54.8	169.8	152.7
28	5.2±3.2	62.4	145.4	118.5
29	4.39±2.4	49.25	210	169.4
GRAND AVERAGE	(6.48±3.2)	72.4	166.6	142.4
31	5.46±3.65	52.4	151.4	139.4
32	4.72±3.25	54.4	195.2	151.4
34	4.45±3.0	58.8	175.8	151.5
35	4.5±3.0	60.4	167.6	156.3
GRAND AVERAGE	(4.8±3.2)	56.5	172.5	149.7

measured dislocation densities are given in Fig. 7A and 7B.

There are two important features to be noticed about this curve;

1) There is no visible nucleation period associated with the formation of the vacancies.

2) At about f(t) = 0.6 there is a departure from a simple exponential function of the form [1 - exp (-t/τ)]. At about this point the fillup rate becomes smaller than predicted by this relation.

In addition we have indicated the maximum possible vacancy contribution from the surface and grain boundaries in Fig. 4. This curve is computed under the assumption that only these two types of sources can produce vacancies and that they are capable of maintaining local equilibrium at all times. The diffusion equation is then solved* for the case of combined radial flow using the value of a for untwinned grains listed in Table II and a cylinder length (L) of 127μ . The plotted solution represents an upper limit to the external source contribution, since the internal sources are neglected in solving the diffusion equation. At the half-time (f = 0.5) the maximum external contribution is only 8.3%, which is an upper bound due to the neglect of the dislocation contribution.

2. Vacancy Generation Kinetics at 878°C

A similar series of experiments are performed at 877.6°C

---

*See Appendix B for the details of the solution.

($\bar{T}_f$) using an initial temperature of 630.6°C ($\bar{T}_i$). The data are reported in Fig. 6, where the maximum external contribution from the surface and the grain boundaries is computed using the value of a listed for the untwinned grains in Table II, $L = 127\mu$ and $D_{1v} = 6.4 \cdot 10^{-6} cm^2 sec^{-1}$.

The curve indicates that the total fill-up time of the lattice is considerably shorter than at 653.3°C, and the extrapolated half-time (f(t) = 0.5) is 9.5 msec as compared to 80 msec at 653.3°C. If only the diffusion of monovacancies from their sources is involved, then the ratio of the half-times is given by,

$$\frac{\tau_{1/2\ (T_1)}}{\tau_{1/2\ (T_2)}} = \exp\left[\frac{E_{1v}^{m}}{k}\left(\frac{1}{T_2} - \frac{1}{T_1}\right)\right] \qquad 4.$$

where $T_2 = 1149.8°K$, $T_1 = 926.46°K$ and $E_{1v}^{m} = 0.85$ eV (Bass and Flynn, 1965). This calculation leads to a theoretical value of 0.126 as compared to an experimental value of 0.12. This lends support to the idea that we are observing a kinetic process limited by the diffusion of single vacancies from their sources, as would be expected for the high temperatures of this investigation.

3. Effect of Grain Size on Generation Kinetics

We have just shown that for the grain size in this experiment the boundaries make a negligibly small contribution to the observed generation kinetics (See Fig. 5 and 6). Therefore, it is interesting to note that Jackson's (1960) early

work on generation kinetics is difficult to interpret in terms of dislocation sources alone because of the fineness of his grain size.* In Table III Jackson's measured half-times ($\tau_{1/2}$) are compared to the grain diam necessary to observe that value of $\tau_{1/2}$ for a spherical grain source model. It is seen that the calculated values range from 26.5μ to 29.8μ. Since Jackson's gold wires** had a diam of only 50.8μ we conclude that the grain size is sufficiently small to allow the grain boundary sources to dominate the generation kinetics. From the present experiment we may give a simple criteria for observing dislocation source effects in the absence of grain boundary source action. The criteria requires the ratio of the grain diam to the interdislocation spacing to be greater than about 200. It is clear that Jackson's experiment does not meet this criteria for an expected nominal density of $10^7 cm^{-2}$.

We also note that the present generation rates agree with those of Lund (1964) and Koehler and Lund (1964) within a factor of about two. Our conclusion that our generation rates are too rapid to be explained by a diffusion limited grain boundary source model agrees with Lund and Koehler's similar conclusion for their large-grained specimens.

---

*The author wishes to thank Dr. P. B. Bowden for bringing this fact to his attention in March 1963.

**Jackson does not state his grain diam so an exact comparison is difficult.

TABLE III

A COMPARISON OF J. J. JACKSON'S (1960) EXPERIMENTAL HALF-TIMES WITH A GRAIN BOUNDARY MODEL

T °C	$D_{lv}.10^7$ ($cm^2 sec^{-1}$)	$\tau_{1/2}$ (measured)	calculated grain diam (μ) which fits measured $\tau_{1/2}$
650	8.2	80	29.8
700	14	40	27.3
800	35.2	15	26.5

C. Control Specimens

To provide a check on the technique used for the dislocation density determinations, specimens are subjected to various treatments, and their dislocation densities are measured. These data are reported in the form of histograms in Fig. 8A-8D.

Specimens 18 and 20 are well annealed and slowly cooled with $\mathcal{R}$ values of 4295 and 3884 respectively. The mean density is $(6.3 \pm 4.1) \cdot 10^7$ cm·cm^{-3} and the resulting distribution is highly skewed towards the lower densities. If one attempts to fit the data to a Poisson distribution* with the measured variance (mean number of dislocations per fixed area of view), the distribution does not fit the experimental data. The measured distribution contains a larger fraction of low dislocation density areas and a smaller fraction of high dislocation density areas than the calculated Poisson distribution. Therefore we conclude that the dislocations are non-randomly distributed in the polycrystalline foils.

To test for the effects of "rough" handling on the measured dislocation densities a specimen is also lightly pulled in tension, by hand, at room temperature and its dislocation density measured. As Fig. 8C indicates, the density is $(1.65 \pm 0.78) \cdot 10^8$ cm·cm^{-3}, which is the highest of any of the measured densities. There is also considerably more spread in the distribution, and the histogram is no longer

---

*This point is discussed more fully in Appendix F.

skewed towards low densities. This result is consistent with the larger value of the variance in this case. This experiment is illustrative in indicating the care that must be taken in handling specimens if meaningful dislocation densities are to be obtained by transmission electron microscopy.

The results of the irradiation experiment with 10^{17} neutrons cm^{-2} are plotted in Fig. 8D. The average density is $(3.17 \pm 2.36) \cdot 10^{7}$ cm cm^{-3}. This is the lowest measured density but the mean is still well within the average deviation of the densities measured for the specimens used in the pulsing experiments (see Fig. 7). This histogram is also skewed towards low dislocation densities and does not fit a Poisson distribution with the measured variance of 4.3. This set of data indicates that densities measured by electron microscopy are satisfactory if one observes the precautions described in article II D1.

The final histogram (8A) is for Specimen 33, which is the pulsed and unquenched specimen whose treatment is outlined in section II E. Its dislocation density is $(4.3 \pm 3.0) \cdot 10^{7}$ cm cm^{-3}, which is within the same range of values as the previously described data. Accompanying this dislocation density are the resistivity data in Fig. 9. The bottom curve (1) serves as a control on the top curve (2) and is for a specimen handled as described in article II E. The average resistivity change per measurement for curve 1 is $1.65 \cdot 10^{-12}$ Ω cm, while for curve 2 it is $4.52 \cdot 10^{-12}$ Ω cm, which is a difference ($\Delta\rho$) of $2.87 \cdot 10^{-12}$ Ω-cm per measurement. If this

value of $\Delta\rho$ is converted to dislocation density from the relation $\Delta\rho/N_d = 2.6 \cdot 10^{-19} \Omega\,cm^3$ (Basinski, Dugdale and Howie, 1963), then $1.1 \cdot 10^7$ cm cm^{-3} of dislocations is introduced per pulse. Assuming this is true, we might then expect a value of about 2.10^8 cm cm^{-3} for the free dislocation density, rather than the measured $(4.3 \pm 3.0) \cdot 10^7$ cm cm^{-3}. That we do not observe the higher value is not surprising as the specimen is annealed at the initial temperature ($\overline{T}_i \sim 430^\circ C$) and also the final temperature ($\overline{T}_f \sim 650^\circ C$) during the bridge balancing operation. Apparently, therefore, the additional dislocations, put in by the pulsing raise the resistivity of the specimen, but do not appreciably affect the measured free dislocation density. This result may be expected, since the extra dislocations undoubtedly polygonize, climb into existing subgrain walls, grow out of the crystal or are annihilated by combining with dislocations of opposite sign during the anneals. We conclude that a small amount of deformation is produced during each electrical pulse, but that the dislocations produced do not contribute cumulatively to the free dislocation density. This is consistent with the observation that reproducible results are obtained in the resistivity work for the same specimen during successive pulses. Our interpretation is supported by the extensive studies of Young and Savage (1964) who find that if N_d is greater than $\sim 10^5$ cm^{-2}, then annealing causes polygonization without large reductions in the total number of dislocations.

D. Deformation Induced as a Result of Electrical Pulsing

We have shown experimentally (Sec. III C) that electrical pulsing results in plastic deformation as a consequence of the Pinch Effect (Northrup, 1907). The deformation occurs during the temperature rise from $\overline{T}_i$ to $\overline{T}_f$, with a generous upper limit of about 10^7 cm^{-2} for the number of dislocations introduced per pulse. It is the purpose of this final section to estimate the pulsing current necessary for deformation to occur and examine the possible consequences of the deformation on the observed generation rates.

If we take the critical shear stress to cause slip as $2.7 \cdot 10^6$ dynes cm^{-2} then the minimum current* to reach this stress is 470 amp, for the foil geometry employed in the present experiment. Currents of this size are possible in the early portions of the pulse, so the resulting deformation (see Sec III C) is certainly consistent with the existence of the Pinch Effect. The effect is a small one ($2.78 \cdot 10^{-12}$ -cm pulse^{-1}), but a very real and important one.

There are several important questions that the deformation raises. For example;

1) How do the extra dislocations introduced during the pulse affect the generation kinetics? Is it possible that a burst of dislocations is injected during the pulse which contributes to the generation rate and then anneals out rapidly enough during the remainder of the pulse to escape final detection?

---

*The derivation of an expression for the critical current to cause slip is presented in Appendix G.

2) How many dislocation jogs are created as a result of dislocation intersection and is this jog concentration an appreciable fraction of the thermal equilibrium jog density?

3) What is the atomic fraction of point defects created by the deformation?

For the low level of deformation involved in this experiment (2) and (3) should be quite small. But (1) can be a significant effect, since the generation half time is inversely proportional to the dislocation density. The possibility that large numbers of dislocations are generated during the pulse and then anneal out during the latter portions of pulse is tested by measuring the dislocation densities for pulsed specimens which are not reannealed at high temperatures (i.e., T less than 100°C). These data are presented in Table IV, and it is seen that each specimen has a density which is within the arithmetic deviation of the grand average for all eight specimens. Therefore, we conclude that for the pulse times of the specimens listed in Table IV no detectable concentration of extra dislocations is present. The fact that the entire generation curve shows a smooth continuous behavior is well understood in terms of the measured dislocation densities and is further evidence that large concentrations of pulse-induced dislocations are not present in the earlier portions of the pulse period. Finally, it is concluded from the resistivity experiments (See Fig. 9 and previous section) that a generous upper limit to the number of residual dis-

TABLE IV

DISLOCATION DENSITY AS A FUNCTION OF PULSE TIME

SPECIMEN NUMBER	T_f °C	t* (ms)	$N_d \cdot 10^{-7}$** ($cm\ cm^{-3}$)
24	652	80	(8 ± 4.85)
25	654	200	(6.89 ± 3.8)
28	658	680	(5.25 ± 3.2)
29	660	745	(4.39 ± 2.4)
31	678.5	220	(5.46 ± 3.55)
32	877.5	100	(4.72 ± 3.25)
34	882.5	150	(4.45 ± 3.0)
35	878.5	230	(4.5 ± 3.0)

$$\text{grand average} = (5.46 \pm 3.38)$$

* t is the time spent by the specimen at T_f.

** The values reported are the arithmetic means and the ± values are the mean deviations.

locations produced per pulse is only about 10^7 cm^{-2}. Hence, it is felt that the measured dislocation densities (see Fig. 7) represent reasonably good average values for the densities in the specimens during the pulses.

IV. DISCUSSION

In the following sections several possible models for the vacancy generation kinetics are discussed. The experimental data are not inconsistent with a diffusion limited dislocation climb model employing a non-random dislocation array. This result forces us to reconsider several current ideas concerning the ease of vacancy production at dislocations.

A. Vacancy Diffusion Limited Dislocation Climb (DLDC)

In DLDC the rate limiting step is the migration of vacancies away from the dislocations into the lattice and not the production of vacancies on the dislocation lines. Thus, we begin by assuming that the vacancy concentration at a distance b* from the core is given by the equilibrium value for $\overline{T}_f$. We also employ a monovacancy diffusion coefficient (D_{1v}) and consider all the flow to be radial. The assumption of monovacancy diffusion is reasonable (Baluffi, Koehler and Simmons, 1963) since the experiments are conducted at T/T_m greater than 0.69. We also neglect all vacancy - dislocation interactions.** A non-random array of dislocations is employed since this type of array is in agreement with the dislocation density data. An exact mathematical analysis based on a non-random array is intractable, so we use the approximation of breaking the lattice up into volume fractions

---

*The parameter b is chosen to be 3A.

**See discussion in Appendix D.

(V_{N_d}) each possessing different dislocation densities. The analytical solution is obtained by assuming that the dislocations are arranged on a regular array in each volume fraction (V_{N_d}). The diffusion equation in each volume fraction is then solved for a single dislocation lying along the axis of a cylinder of inner radius b and outer radius R, where 2R is given by $(N_d)^{-1/2}$. We also require that there is no flux of vacancies between cylinders. The resulting* solution is:

$$f = \frac{\bar{C}(t) - C_i}{C_o - C_i} = 1-\exp\left(-\xi D_{1v} N_d t\right) \qquad 5.$$

where ξ is a geometrical factor and t is the time. Therefore the analytical solution for the multi-volume model is a sum of terms of the form of Eq.(5) weighted by a volume fraction for each dislocation density. A mathematical statement of this is given by,

$$f^1(t) = \sum_{V_{N_d}} V_{N_d} \left(1-e^{-\xi N_d D_{1v} t}\right) \qquad 6.$$

where V_{N_d} is the volume fraction of the lattice occupied by the dislocation density N_d.

Our procedure is now to attempt to fit the observed generation curves to the above model. We employ dislocation distributions possessing a total density within the measured range and non-random distributions which are not inconsistent with the measured non-Poisson form of the distributions. A

---

*See Appendix D.

A distribution that is found to fit both sets of experimental data is;

N_d (cm^{-2})	v_{N_d}
$5 \cdot 10^6$	0.60
$10 \cdot 10^6$	0.30
$30 \cdot 10^6$	0.10

This distribution has an average N_d ($9 \cdot 10^6$) which is barely within the range of uncertainty of the measured values. The resulting curves (II) are plotted in Fig. 10 and 11 along with the best fit experimental data given in Fig. 5 and 6. It is seen that the above distribution fits the experimental data at all times within the indicated error bands.

We may use all of the experimental data to define a vacancy generation efficiency at the dislocation. If we define the average generation efficiency N as

$$N = \frac{\text{measured generation rate}}{\text{generation rate predicted by DLDC for measured } N_d} \quad 7.$$

We obtain the following results:

N (878°C) = 0.19

N (653°C) = 0.14

N (Irradiated) = 0.29

The average efficiency based on all the measured average dislocation densities*, is therefore about 0.21. This result

*It is interesting to note that the mean value of these three distributions (see Fig. 7 and 8D) have a range from $3.17 \cdot 10^7$ cm cm^{-3} to $6.48 \cdot 10^7$ cm cm^{-3} which is only a factor of 2 in spread. Since the distributions are determined from 11 different specimens this small spread in the mean values increases our faith in the measuring technique.

indicates, that the dislocations operate as very effective sources. It is strongly emphasized that the efficiency (N) is an average value for the entire dislocation distribution.

In all the previous statements on dislocation efficiency it is tacitly assumed that all types of dislocations should emit vacancies with the same ease. This is most likely not the actual case and the edge and screw character (Thomson and Balluffi, 1962, Escaig, 1963, Friedel, 1964) of the dislocation should be taken into account. It is quite conceivable that certain dislocations climb more easily and with higher efficiencies than the average efficiency for the entire distribution. Therefore we emphasize that our efficiencies are average values for a dislocation density distribution that has an unspecified character with regard to both the type and the climb ability of its members.

A common approach in treating the diffusion of point defects from or to dislocations is to invoke a regular or random dislocation array. These types of arrays are not in accord with the measured non-Poisson nature of the dislocation distributions, and hence it is not surprising that present attempts to fit the experimental data to Eq. (5) for a fixed N_d have not been successful.

We conclude this section on DLDC with the following summary;

1) The dislocations act as very effective vacancy sources. The generation rate data can be fitted using a DLDC model employing a non-random dislocation distribution

which is not inconsistent with the measured dislocation distributions. However, the total densities required are barely within the lower limit of the range of uncertainty of the measured densities.

2) If we use the average dislocation density for all the measured dislocation distributions, then we may conclude that <u>average</u> generation rate occurs at a rate which is <u>about 0.2</u> of the generation rate calculated on the basis of <u>DLDC</u>.

<u>B. Vacancy Production Limited Dislocation Climb (PLDC)</u>

Since the <u>average generation efficiency</u> is about 0.2, then the <u>average</u> rate of vacancy production at dislocations is possibly rate controlling. It is therefore of interest to discuss various models dealing with the rate of vacancy production at dislocation cores.

The treatment of vacancy induced climb is usually couched in terms of jogs, where the vacancies may be easily created or destroyed (e.g. Mott, 1951, Weertman, 1955, 1957, Lothe, 1960, Thomson and Balluffi, 1962, Friedel, 1964). The continuous production of vacancies will cause existing jogs to diffuse along the dislocation cores towards eventual annihilation. In order to maintain a quasi-steady state new jogs must be continuously nucleated. Thus the climb rate may become controlled by the ease of jog nucleation and the jog formation energy is the dominant factor to be considered. In the present discussion homogeneous jog nucleation will refer to spontaneous jog formation along relatively straight

unperturbed sections of the dislocation line. On the other hand, heterogeneous nucleation will refer to jog nucleation at special sites (i.e. nodes,highly stressed regions, etc.). It is emphasized that this section is of a more speculative nature than the preceding one, as there is no a priori manner of distinguishing between heterogeneously and homogeneously formed jogs.

1. Vacancy Production at Heterogeneously Formed Jogs

An objection to any homogeneous climb model is that heterogeneous nucleation of jogs at the nodal points of the dislocation network may always outstrip the homogeneous nucleation on the straight portions of the dislocation lines. Thomson and Balluffi (1962) discuss this problem in their treatment of homogeneous climb and conclude that as long as the distance between jogs established by homogeneous process is small compared to the dimensions of the climbing dislocation line, then homogeneous climb will be dominant. This conclusion implies a low jog energy in general, since the distance between jogs tends to decrease with decreased jog energy. Thus the important question to answer is how large may the jog energy (ε_j) become before the heterogeneous nucleation rate at the nodal points becomes comparable to the homogeneous nucleation rate along the dislocation line. But it is this question that is difficult to answer since the calculation of the heterogeneous jog density is well beyond our present capabilities. Therefore we will proceed to the case of homogeneous nucleation, since we may deal with this problem semi-

quantitatively.

2. Vacancy Production at Homogeneously Formed Jogs

The problem of homogeneous climb of a straight unconstrained pure edge dislocation has been treated by Thomson and Balluffi (1962). Their theory predicts the climb rate and the jog density of an edge dislocation under the conditions of DLDC and PLDC in the presence of a subsaturation (S) of vacancies. In both DLDC and PLDC the climb rate and the jog density depend on the degree of subsaturation, the jog energy and the distance (α^{-1}) a vacancy will travel on an unjogged dislocation before jumping off. The subsaturation (S) is related to our measured parameter f by

$$S = f-1, \qquad 8.$$

thus we have experimentally measured S as a function of time. The subsaturation is also a measure of the chemical potential (free energy per vacancy), which is given by

$$\mu_v = kT \ln f = kT \ln (S + 1). \qquad 9.$$

Physically S is a measure of how far from equilibrium the lattice is and is therefore a measure of the driving force for climb. As the vacancy sources generate vacancies $|S|$ decreases and the driving force for climb decreases correspondingly. Thus for a lattice deficient in vacancies S may range from -1 to 0 depending on how far the specimen is from its equilibrium vacancy concentration. The free energy per vacancy (μ_v) is the work available to take an atom from the crystal and place it on the surface, thereby creating a vacancy. It is seen that for values of S near -1 the avail-

able free energy becomes very large while for S=0, μ_v is zero.

For DLDC the equilibrium jog density (L_o^{-1}) is independent of the subsaturation, while for PLDC the jog density (L^{-1}) is a function of the subsaturation and decreases as the subsaturation decreases. In addition the climb rate in PLDC is directly proportional to the jog density and therefore also decreases as the subsaturation decreases. Thus the measured parameter S is intimately connected with the kinetics of dislocation climb. Since S and μ_v are so important physically it is of interest to examine the behavior of μ_v as a function of f=(S + 1). This is done in Fig. 12 where we plot the chemical potential for an upquench from 436.2°C ($\overline{T}_i$) to 653.3°C ($\overline{T}_f$) versus f and also for a downquench from 653.3°C (Tq) to 60°C (T_a). Note the rapid manner in which the chemical potential dies off for the upquenched specimen as it equilibrates, while it remains essentially constant for the downquenched specimen during the entire annealing process. The asymmetry of the chemical potential noted in these two cases may contribute to the apparent effective dislocation sink action for heavily supersaturated vacancies in quenched gold (Seidman and Balluffi, 1964).

If the generation efficiency is close to unity, then climb will be essentially diffusion limited and we may estimate the energy to form a jog (ε j) from the condition

$$\alpha L_o < 3. \qquad 10.$$

This equation is the Thomson-Balluffi (1962) criteria for DLDC during the entire generation process and predicts an upper

bound to the jog energy of about 0.6 eV. It is interesting to note that for a completely DLDC model the jog density (L_o^{-1}) is unperturbed by the decrease in |S|. We re-emphasize that the $\mathcal{E}_j$ of 0.6 eV is obtained under the assumption of continuous homogeneous jog nucleation and the condition that the actual generation efficiency is close to unity during the entire climb process.

A quantitative treatment of PLDC is even more difficult than DLDC, since we must specify the convergence length (Λ') of a well formed jog in addition to the parameters just discussed. The mode of climb may become production limited if the jog energy is greater than about 0.6 eV. For a particular jog energy ~~energy~~ and convergence length there is a critical subsaturation* at which climb becomes production limited. The larger the jog energy (for a fixed convergence length) the larger the value of |S| when the climb becomes production limited. If the jog energy is large enough the entire process is production limited and even an S of about -1 is not large enough to force the system into DLDC. For intermediate jog energies the generation process could be a combination of PLDC and DLDC. In view of our present lack of knowledge of the values of the parameters governing homogeneous climb it is best to leave the problem of PLDC with the result that climb will be partially production limited for a jog energy greater than about 0.6 eV and can be totally production

---

*See Appendix E for the detailed formulae.

limited for any value of S if the proper combination of jog energy ($\mathcal{E}_j$) and convergence length (Λ') is present.

C. Comparison of the Present Results with the Previously Determined Jog Energies

The present state of knowledge of jog energies in face centered cubic metals is in a rather poor state. The situation is particularly bad for the low stacking fault energy metals, like gold, where the equilibrium jog configuration is not even known.* For example, on the theoretical side Seeger (1955) has estimated the jog energy of an edge dislocation in copper to be 4.2 eV. However, Friedel (1964) estimated the jog energy to be only $1/10\,\mu b^2 d$ (0.92 eV in gold). Here μ is the shear modulus, b the magnitude of the Burgers' vector of the partial dislocations and d the equilibrium spacing of the partial dislocations. Recently Escaig (1963) has proposed several models for the climb of extended dislocations (see also Thomson and Balluffi, 1962) and claims that a dissociated edge dislocation will climb when μ_v is 0.40 eV while partial screw dislocations will climb when μ_v is 0.65 eV. On the experimental side Thorton and Hirsch (1958) estimate $\mathcal{E}_j$ to be 0.65 ± 0.25 eV from a combination of creep and flow stress data at 300°K. Though Seeger (1955) from high

---

*In a low stacking fault energy material the dislocation is dissociated into two partial dislocations separated by a ribbon of stacking fault. See Cottrell (1953) for further details. This makes the problem of determining the jog configuration particularly difficult (Hirsch, 1962).

temperature creep data has estimated the jog energy to be twice Q_1 ($\sim$ 3.66 eV).

If one interprets the present data on a homogeneous climb model and considers the climb to be essentially diffusion limited (DLDC) then as we have seen $\mathcal{E}_j \leqq 0.6$ eV. Thus the present experiment points to rather low jog energies if the homogeneous climb model is valid. It is also interesting to note that if the jog energy in a low stacking fault energy metal like gold is as low as 0.6 eV then jog nucleation should not be a serious problem in a high stacking fault energy metal like aluminum. Thus one would expect dislocations in aluminum to climb quite readily at temperatures where the diffusion coefficients are equivalent to those for gold in the present experiments.

We conclude Sec. B with the following summary;

1) It is difficult to make an apriori decision as to whether the vacancies are formed at homogeneously or heterogeneously nucleated jogs.
2) If climb occurs homogeneously and by a vacancy DLDC process then the jog energy is less than 0.6 eV.
3) Vacancy PLDC climb may occur if the jog energy is greater than about 0.6 eV. The subsaturation at which PLDC will dominate the climb process is a function of the jog energy and the convergence length of the jog. Since the present experiment indicates an <u>average</u> generation efficiency of 0.2 the dominant mode of climb is possibly PLDC with an $\mathcal{E}_j$ of about 0.6 eV or greater.

FIGURE CAPTIONS

Figure 1. Electrical circuit for pulsing polycrystalline specimens.

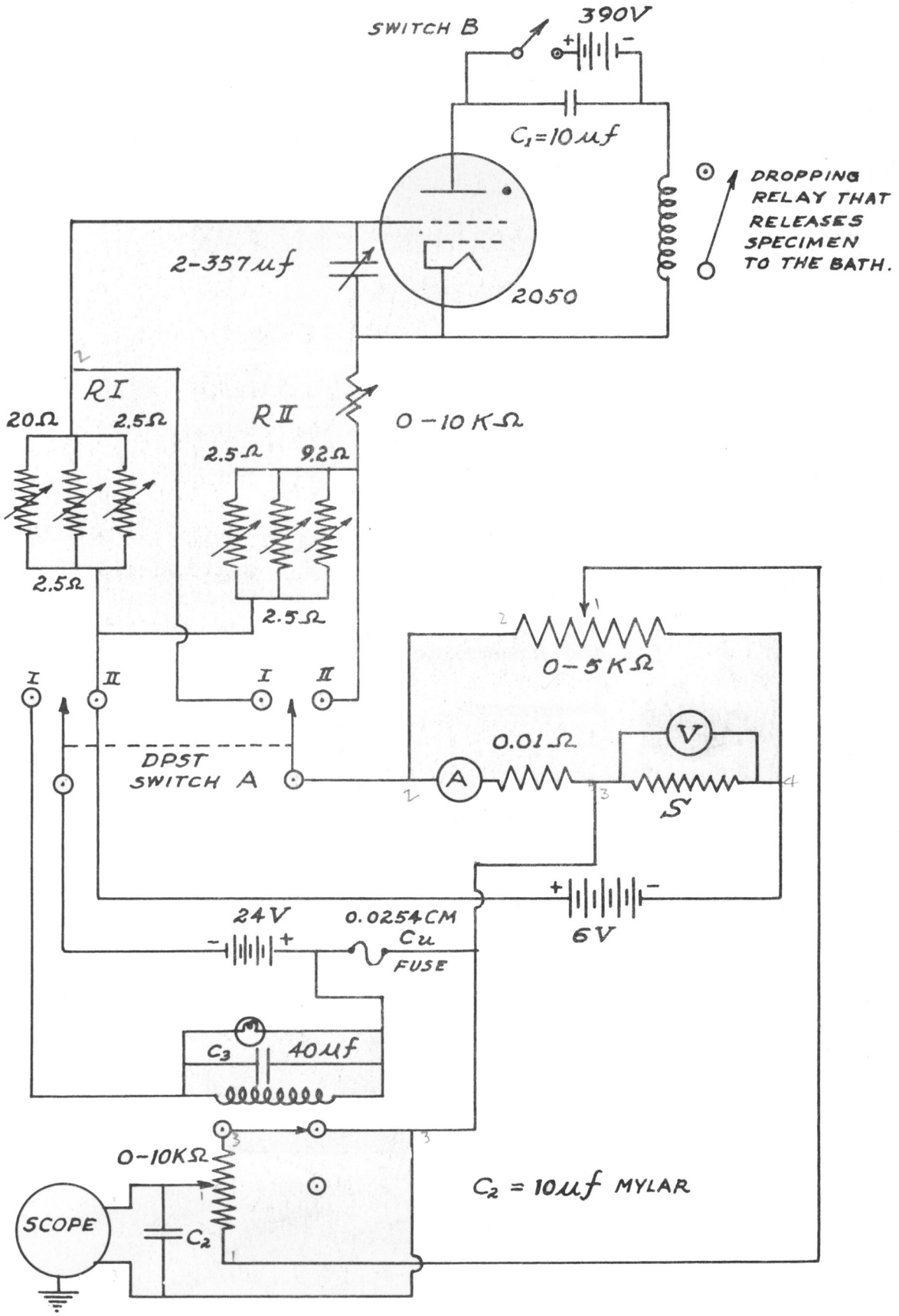
SWITCH B
390V
C_1=10μf
DROPPING RELAY THAT RELEASES SPECIMEN TO THE BATH.
2-357μf
2050
RI
20Ω
2.5Ω
2.5Ω
RII
2.5Ω
9.2Ω
2.5Ω
0-10KΩ
0-5KΩ
I
II
I
II
DPST SWITCH A
0.01Ω
A
V
S
24V
0.0254CM Cu FUSE
6V
C_3
40μf
0-10KΩ
SCOPE
C_2
C_2 = 10μf MYLAR

Fig. 1

Figure 2. Oscillograms of; a) an electrical pulse and downquench; b) a thermal pulse and downquench.

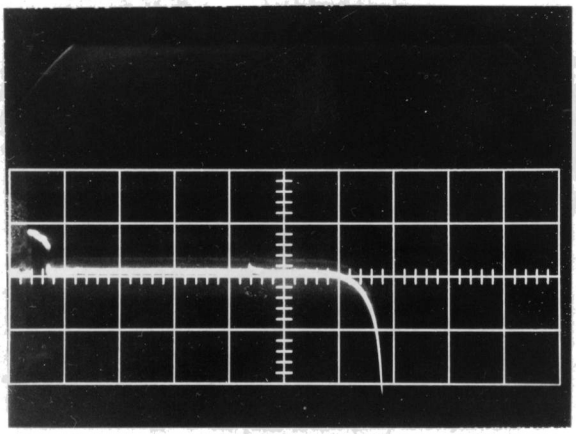

5 mV/cm
7.5°C/cm

A

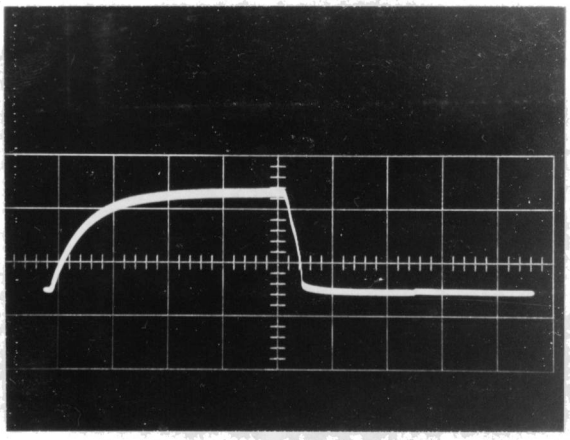

Single crystal
see pp 8 ~9

B

Fig. 2

Figure 3. Schematic diagram of apparatus used to thermally pulse gold single crystals.

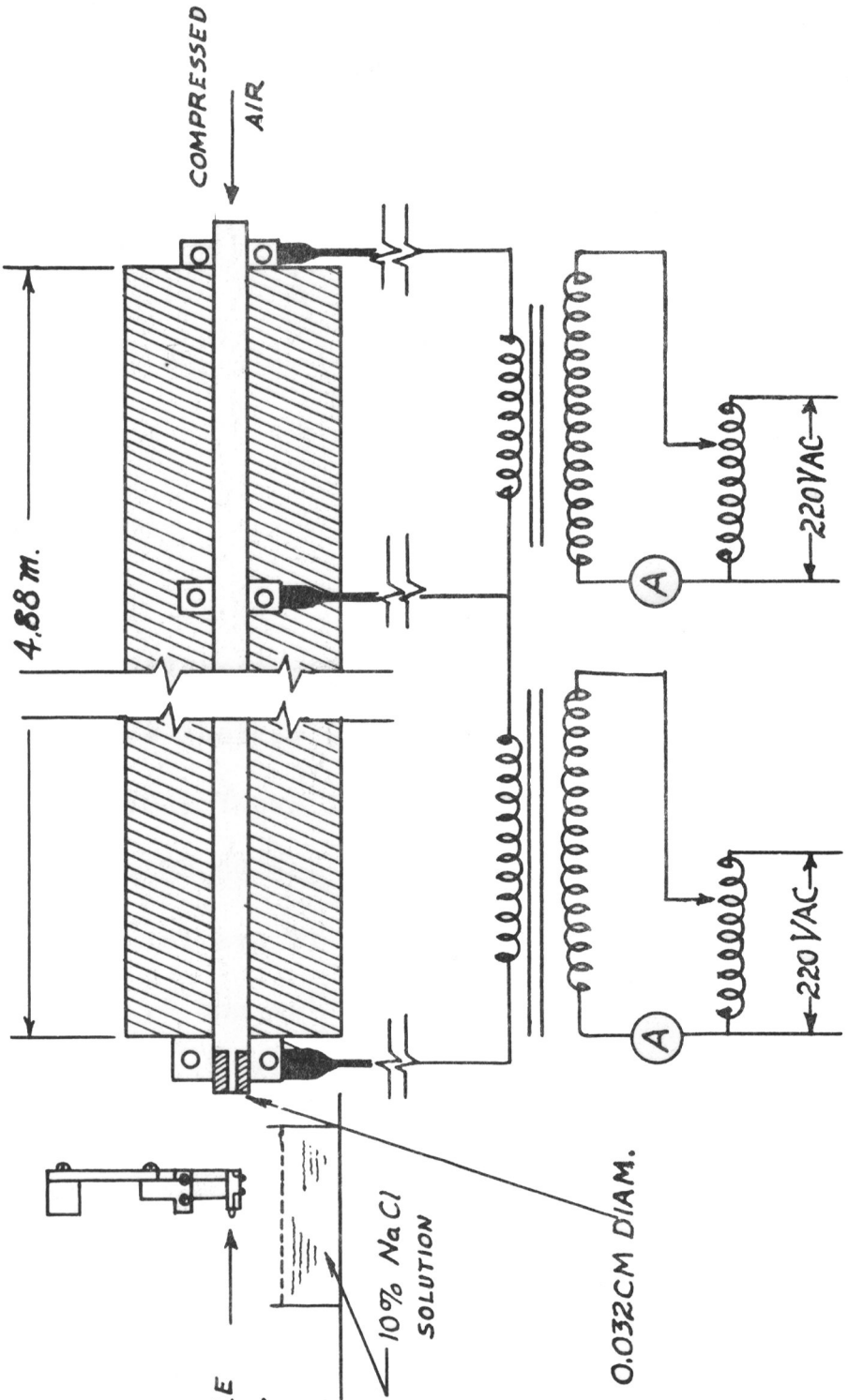
COMPRESSED AIR
4.88 m.
220 VAC
220 VAC
A
A
GOLD SINGLE CRYSTAL
10% Na Cl SOLUTION
0.032CM DIAM.

Fig. 3

Figure 4. Mean vacancy concentration [$\bar{c}$ (t)/C_o] versus time for various vacancy sources. Curves I and II are for 0.0508 cm thick slabs at 875°C and 900°C respectively. Curves III and IV are for subgrains of radius $12.7 \cdot 10^{-3}$cm and $6.35 \cdot 10^{-3}$cm respectively at 875°C. Curve V is for a dislocation density of 10^{7}cm^{-2} at 875°C.

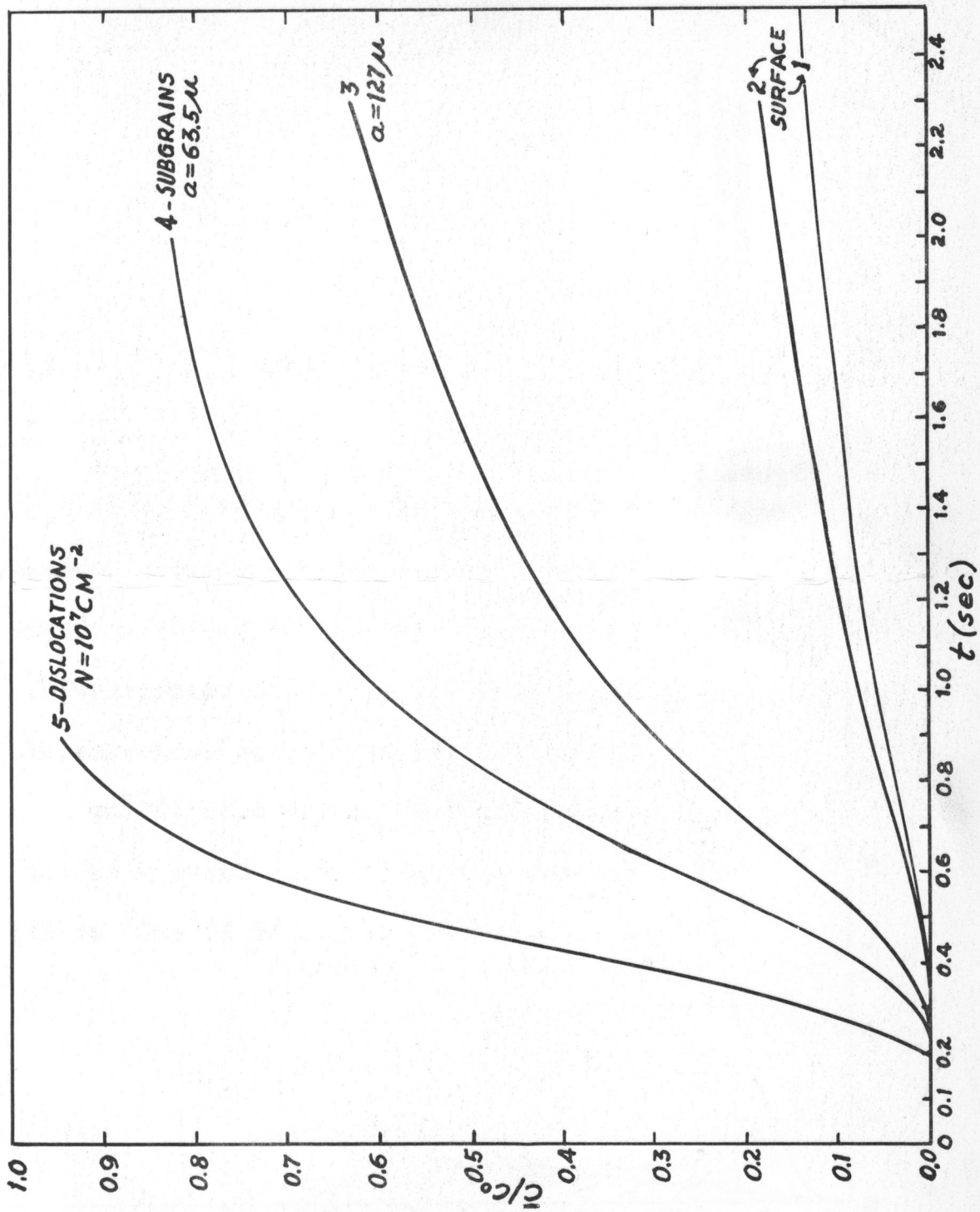
5-DISLOCATIONS
N=10⁷CM⁻²
4-SUBGRAINS
a=63.5μ
3
a=127μ
2
SURFACE
1
C/C₀
t (sec)
1.0
0.9
0.8
0.7
0.6
0.5
0.4
0.3
0.2
0.1
0.0
0
0.1
0.2
0.4
0.6
0.8
1.0
1.2
1.4
1.6
1.8
2.0
2.2
2.4

Fig. 4

Figure 5. f versus t (sec) for $\bar{T}_f$ = 653.3°C and $\bar{T}_i$ = 436.2°C. Electrical pulsing technique.

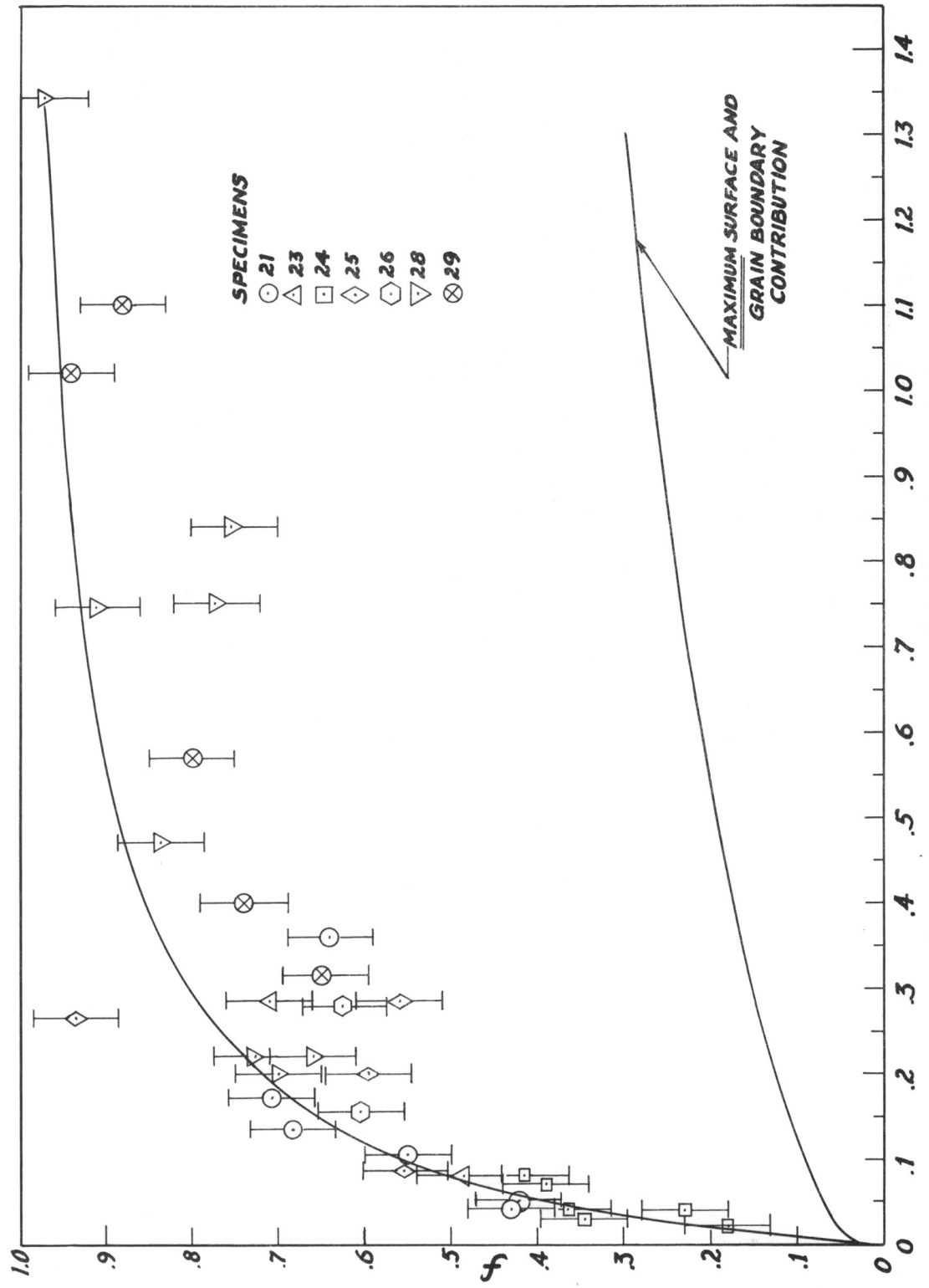
SPECIMENS
21
23
24
25
26
28
29
MAXIMUM SURFACE AND GRAIN BOUNDARY CONTRIBUTION
f
t (SEC)
0
.1
.2
.3
.4
.5
.6
.7
.8
.9
1.0
1.1
1.2
1.3
1.4

Fig. 5

Figure 6. f versus t (sec) for $\bar{T}_f$ = 877.6°C and $\bar{T}_i$ = 630.6°C. Electrical pulsing technique.

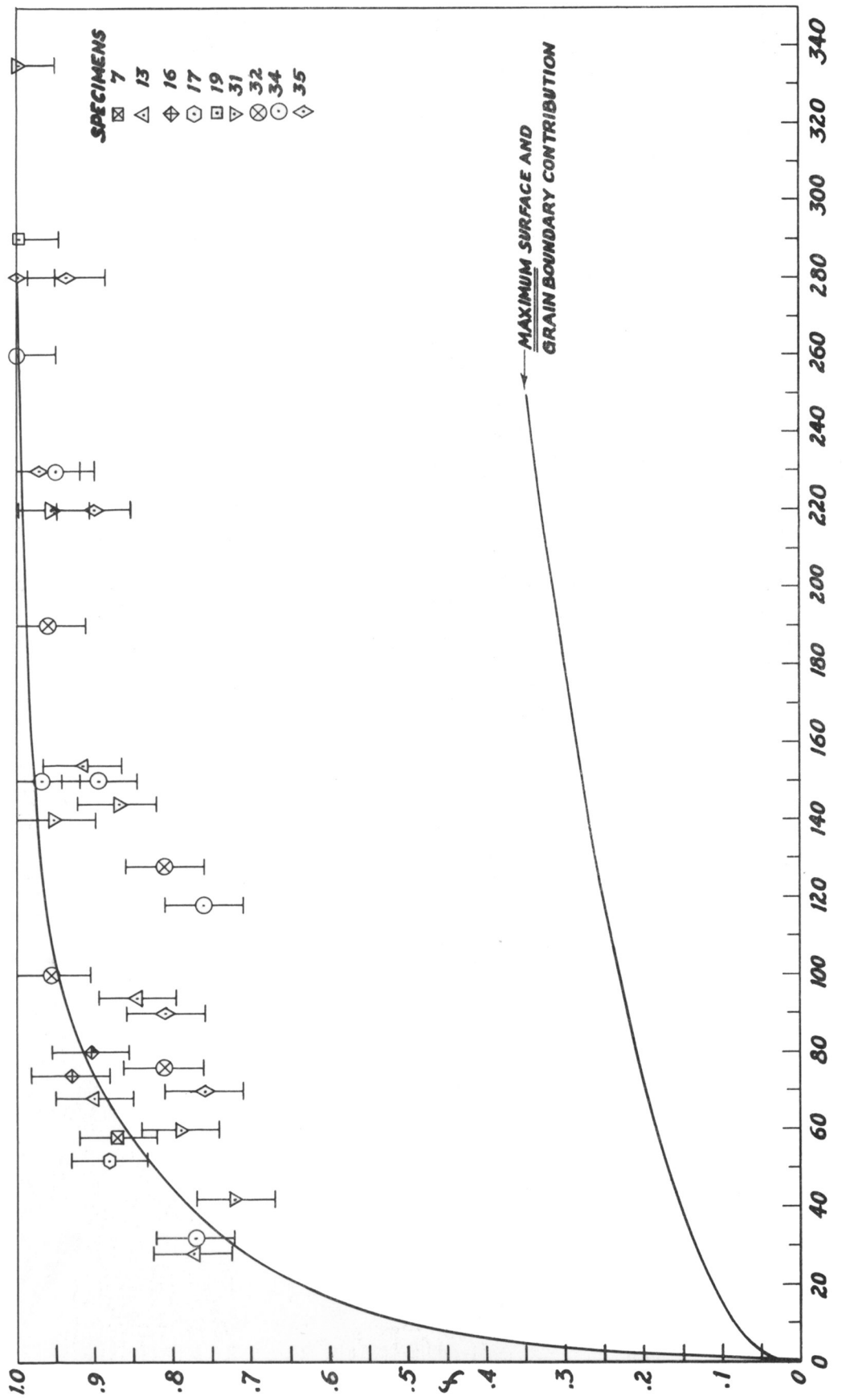

Fig. 6

Figure 7. Histograms of dislocation densities for specimens pulsed to 877.6°C and 653.3°C. The ordinate F is the fraction of the total photographic plates with a dislocation density N_d.

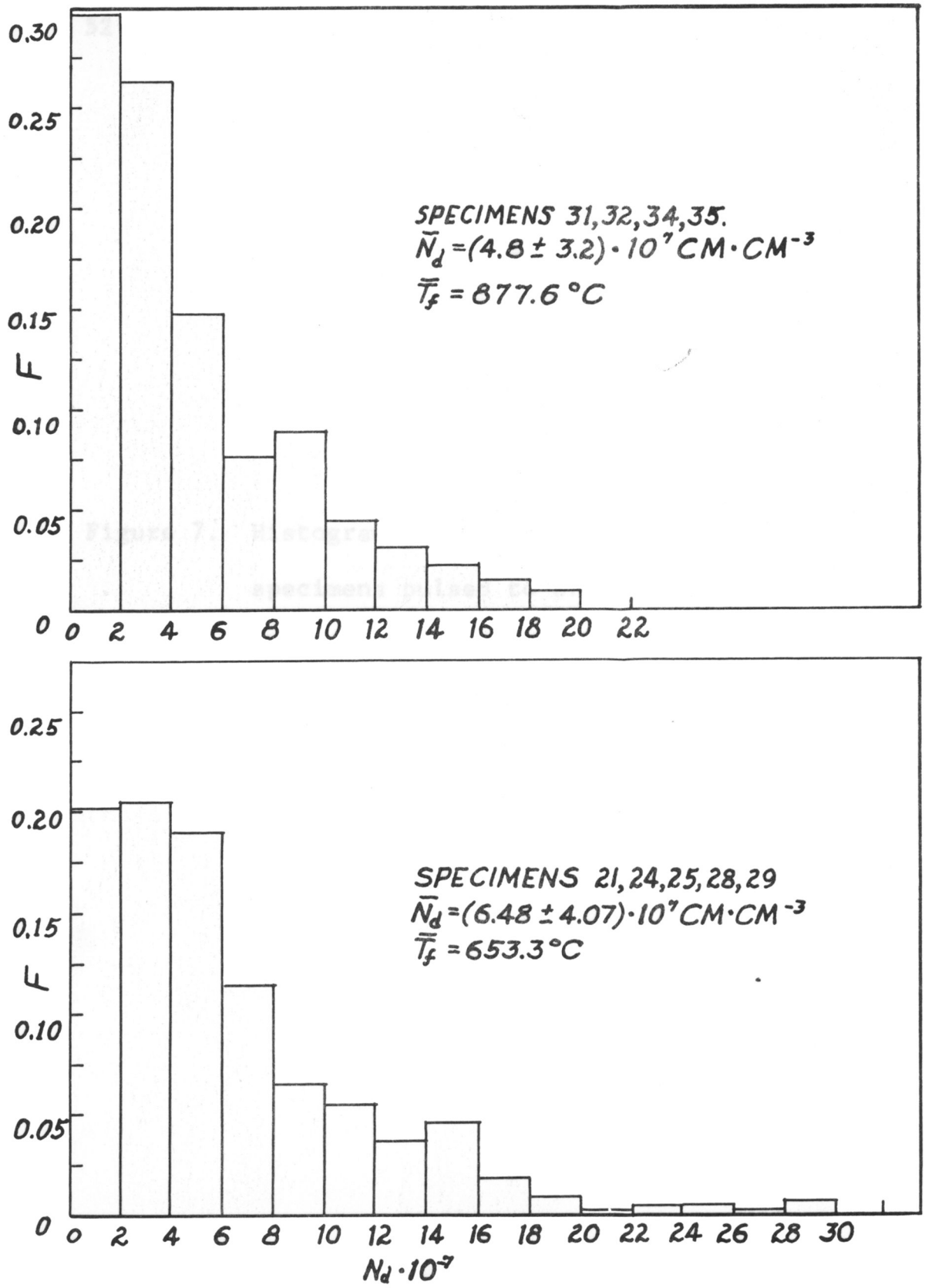
SPECIMENS 31,32,34,35.
$\bar{N}_d = (4.8 \pm 3.2) \cdot 10^7 CM \cdot CM^{-3}$
$\bar{T}_f = 877.6\,^{\circ}C$
F
0.30
0.25
0.20
0.15
0.10
0.05
0
0 2 4 6 8 10 12 14 16 18 20 22
SPECIMENS 21,24,25,28,29
$\bar{N}_d = (6.48 \pm 4.07) \cdot 10^7 CM \cdot CM^{-3}$
$\bar{T}_f = 653.3\,^{\circ}C$
F
0.25
0.20
0.15
0.10
0.05
0
0 2 4 6 8 10 12 14 16 18 20 22 24 26 28 30
$N_d \cdot 10^{-7}$

Fig. 7

Figure 8. Histograms of dislocation densities for for various control specimens. Graph A is for spec. 33 which was pulsed but not quenched. Graph B is for two well annealed gold specimens. Graph C is for a specimen deformed lightly in tension. Graph D is for two specimens irradiated to 10^{17}nvt (fast neutrons).

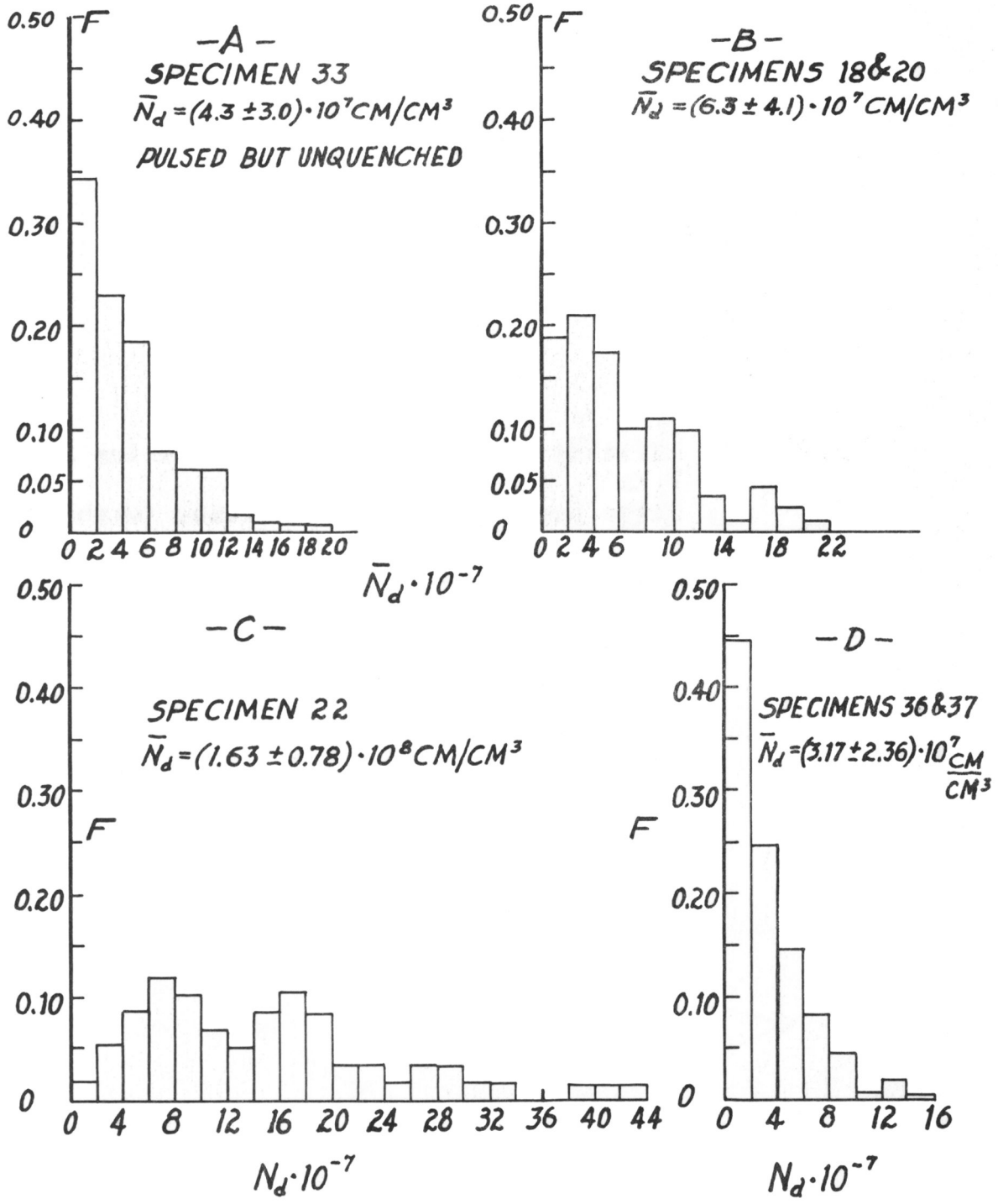
-A-
SPECIMEN 33
$\bar{N}_d = (4.3 \pm 3.0) \cdot 10^7 CM/CM^3$
PULSED BUT UNQUENCHED
-B-
SPECIMENS 18&20
$\bar{N}_d = (6.3 \pm 4.1) \cdot 10^7 CM/CM^3$
$\bar{N}_d \cdot 10^{-7}$
-C-
SPECIMEN 22
$\bar{N}_d = (1.63 \pm 0.78) \cdot 10^8 CM/CM^3$
-D-
SPECIMENS 36&37
$\bar{N}_d = (3.17 \pm 2.36) \cdot 10^7 \frac{CM}{CM^3}$
F
0.50
0.40
0.30
0.20
0.10
0.05
0
0 2 4 6 8 10 12 14 16 18 20
0 2 4 6 10 14 18 22
0 4 8 12 16 20 24 28 32 36 40 44
0 4 8 12 16
$N_d \cdot 10^{-7}$

Fig. 8

Figure 9. Resistivity changes due to handling and also due to electrical pulsing (without quenching). The quantity $\Delta\rho_b$ is the change in the 4.2°K resistivity after a cycle.

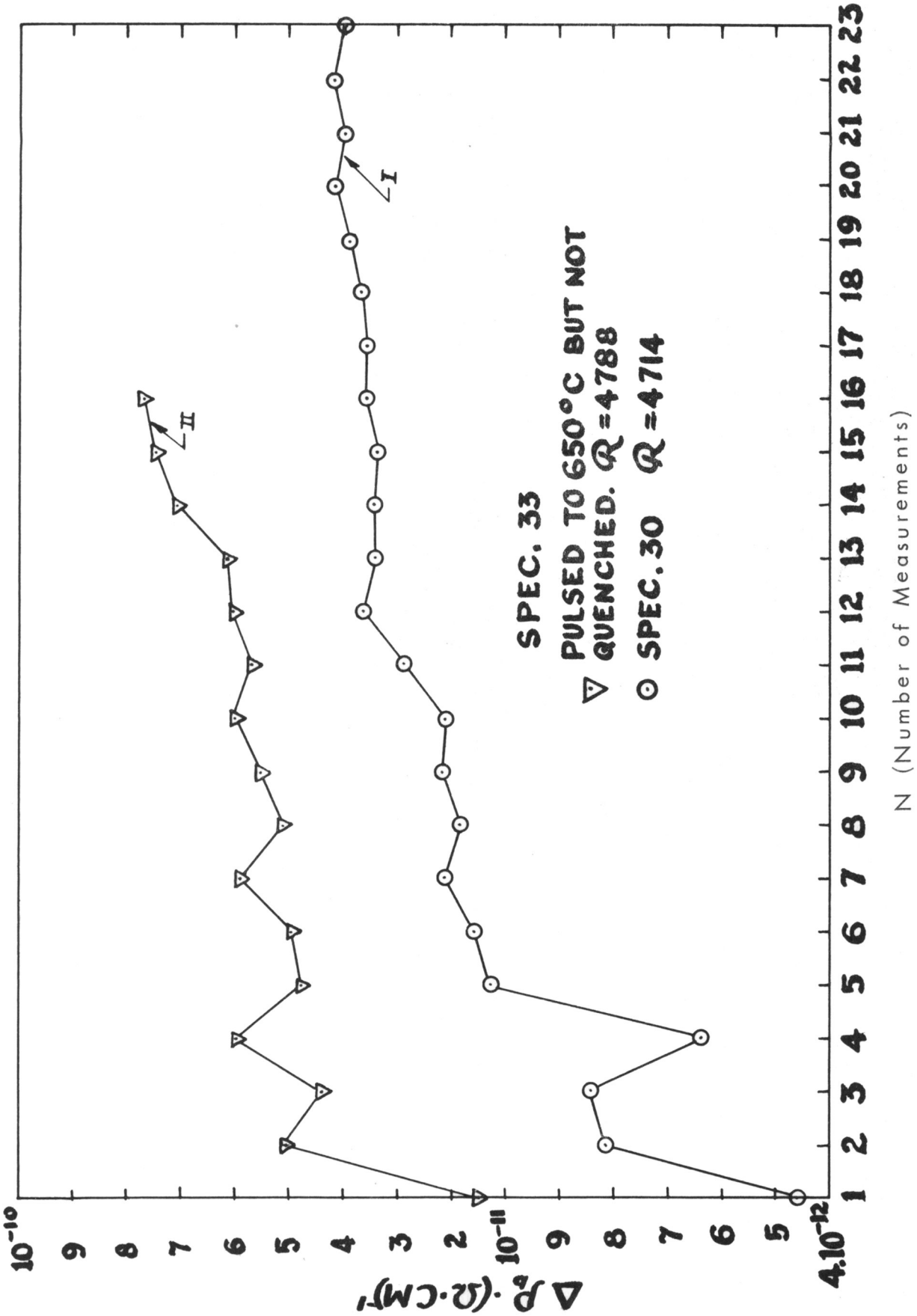
SPEC. 33
PULSED TO 650°C BUT NOT QUENCHED. ℛ=4788
SPEC. 30 ℛ=4714
I
II
Δρ·(Ω·CM)
N (Number of Measurements)

Fig. 9

Figure 10. A comparison of the best fit of the theoretical three volume model with the experimental data ($\bar{T}_f$ = 653.3°C).

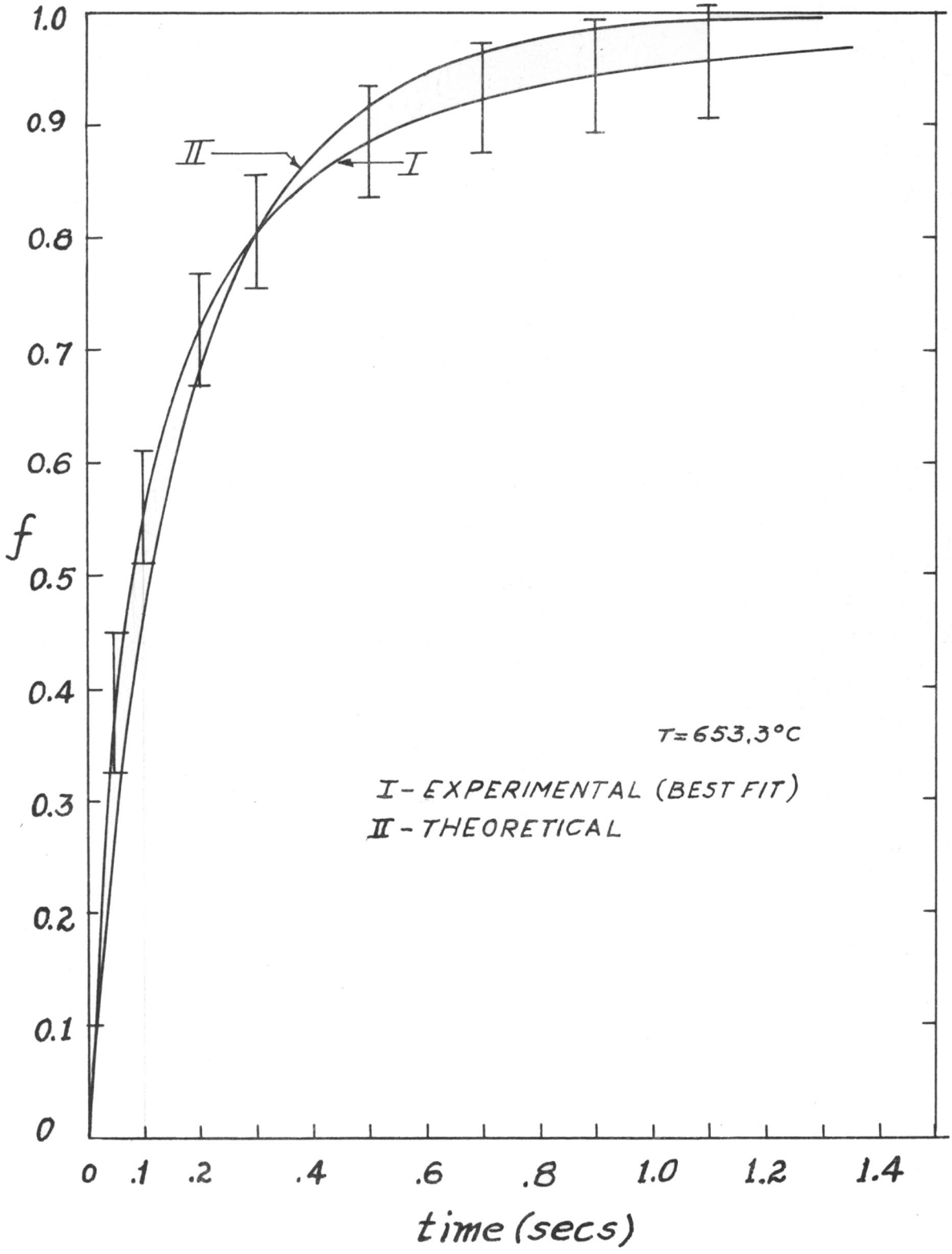
1.0
0.9
0.8
0.7
0.6
f
0.5
0.4
0.3
0.2
0.1
0
II
I
T=653.3°C
I - EXPERIMENTAL (BEST FIT)
II - THEORETICAL
0 .1 .2 .4 .6 .8 1.0 1.2 1.4
time (secs)

Fig. 10

Figure 11. A comparison of the best fit of the theoretical three volume model with the experimental data ($\bar{T}_f$ = 877.6°C).

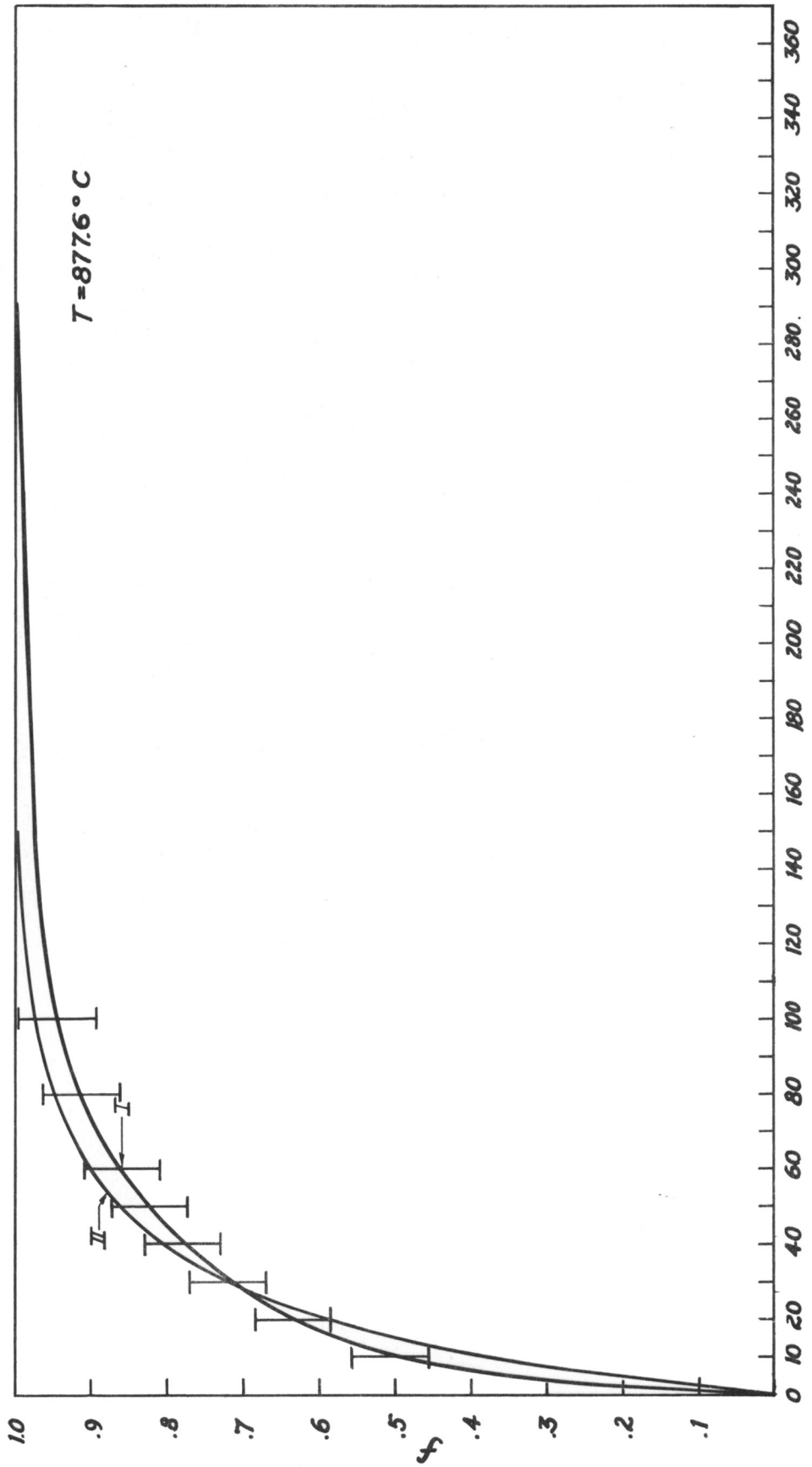
T=877.6° C
I
II
f
TIME (MSEC)
0 10 20 40 60 80 100 120 140 160 180 200 220 240 260 280 300 320 340 360
.1 .2 .3 .4 .5 .6 .7 .8 .9 1.0

Fig. 11

Figure 12. The vacancy chemical potential, μ_v, as a function of f for an upquench from 436.2°C to 653.3°C and also for a downquench from 653.3°C to 60°C. For the upquench f is the fraction of vacancies destroyed.

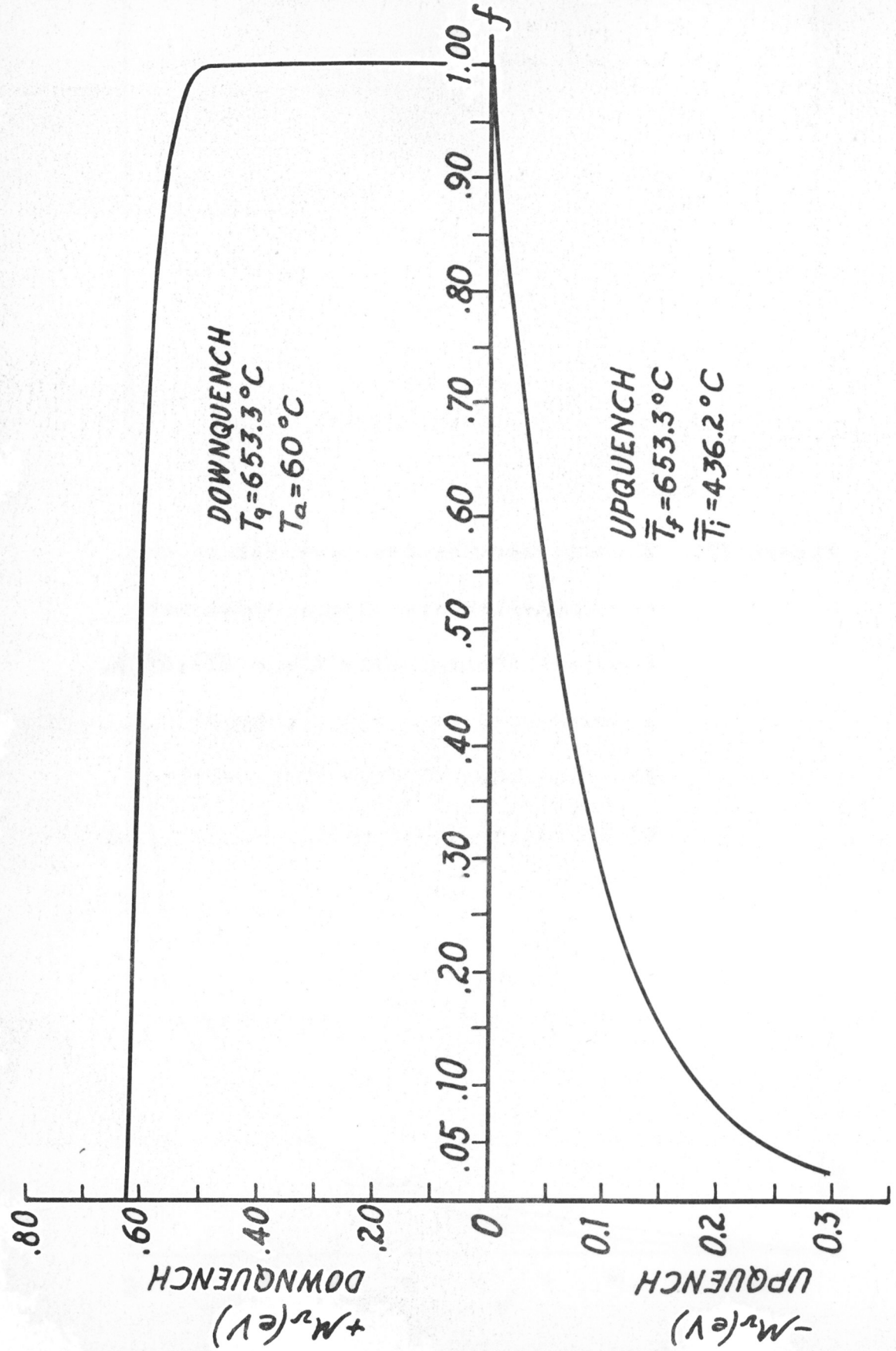
DOWNQUENCH
T_q=653.3°C
T_a=60°C
UPQUENCH
$\bar{T}_f$=653.3°C
$\bar{T}_i$=436.2°C
f
1.00
.90
.80
.70
.60
.50
.40
.30
.20
.10
.05
0
0.1
0.2
0.3
.20
.40
.60
.80
$+M_v$(eV)
DOWNQUENCH
$-M_v$(eV)
UPQUENCH

Fig. 12

Figure 13. A comparison of the isothermal solution with the time and temperature dependent solution for dislocation source behavior. Curve I is the isothermal solution. Curve II is the computed time dependent solution given by Eq. (A.16) with $\alpha = -10.0\ sec^{-1}$. Curve III is also computed from Eq. (A.16) and is for $\alpha = -5.5\ sec^{-1}$. The dislocation density is $10^7 cm^{-2}$, $\bar{T}_f$ is 875°C and $\bar{T}_i$ is room temperature.

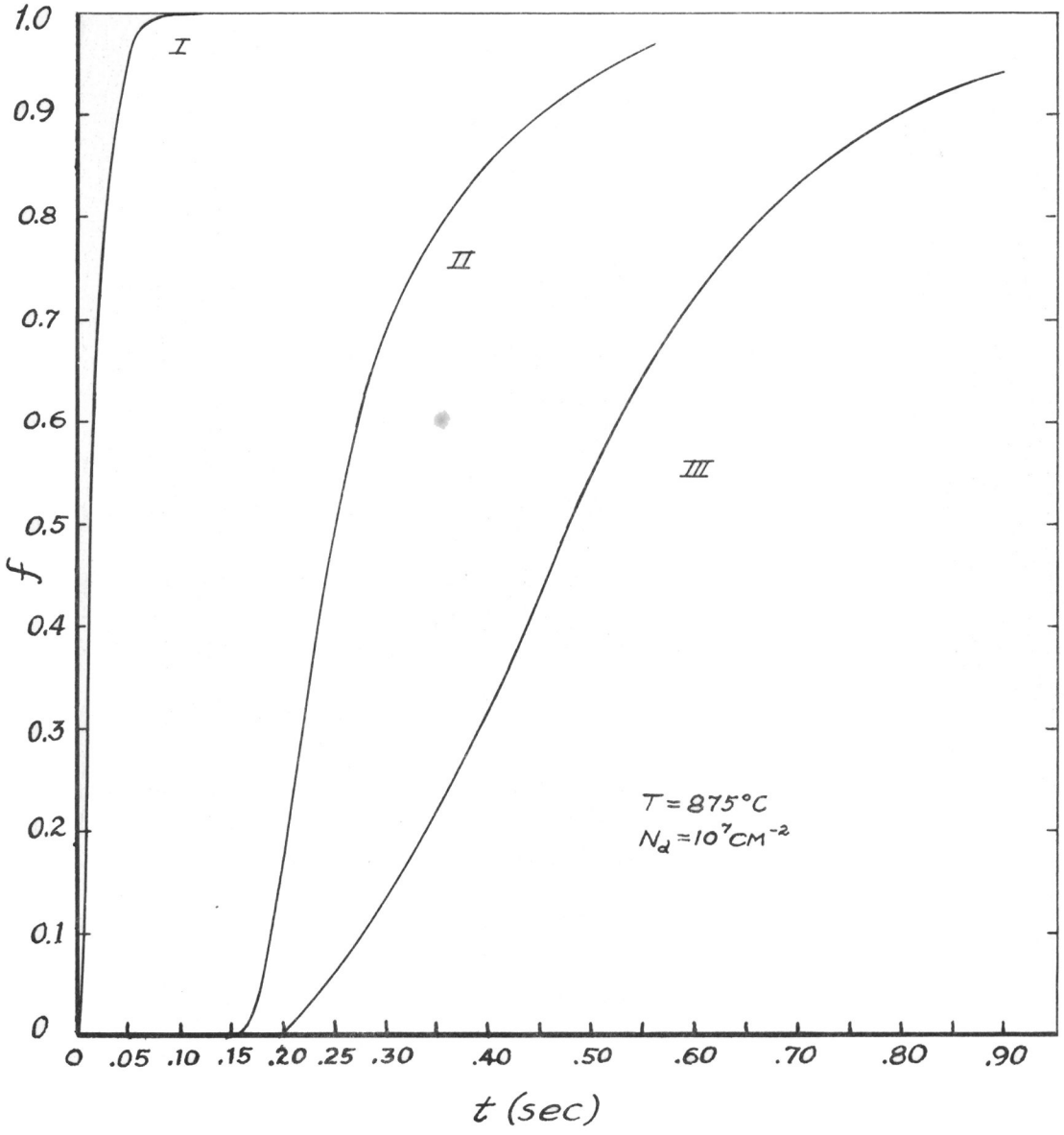
1.0
0.9
0.8
0.7
0.6
0.5
0.4
0.3
0.2
0.1
0
f
I
II
III
T = 875°C
$N_d = 10^7 CM^{-2}$
0 .05 .10 .15 .20 .25 .30 .40 .50 .60 .70 .80 .90
t (sec)

Fig. 13

APPENDIX A

THE SOLUTION OF THE DIFFUSION EQUATION WITH A TEMPERATURE DEPENDENT DIFFUSION COEFFICIENT AND TIME DEPENDENT EQUILIBRIUM BOUNDARY CONDITIONS

In III A we have discussed curves (see Fig. 4) which are obtained from a solution of the diffusion equation. This following equation is solved for a temperature dependent diffusion coefficient and time dependent equilibrium boundary conditions:

$$\frac{\partial C}{\partial t} = \nabla \cdot (D_{lv} \nabla C), \qquad \text{A.1}$$

where $D_{lv} = D_{lv}(t)$, so that A.1 becomes

$$\frac{\partial C}{\partial t} = D_{lv}(t) \nabla^2 C. \qquad \text{A.2}$$

the function $D_{lv}(t)$ is given by

$$D_{lv}(t) = D_{olv} \exp\left[-E^{M}_{lv}/kT(t)\right] \qquad \text{A.3}$$

and T(t) is given by Eq. (1). It is helpful to transform Eq. (A.3) according to

$$t' = \int_0^t D_{lv}(t)\, dt \qquad \text{A.4}$$

so that the equation to be solved is

$$\frac{\partial C}{\partial t'} = \nabla^2 C. \qquad \text{A.5}$$

The mathematical solution to the diffusion equation with time dependent surface conditions and zero initial concentration within the body is found in the statement of Duhamel's

Theorem (Carslaw and Jaeger, 1959, Hildebrand, 1964). This theorem states that for the above conditions the concentration [C(x,t')] is given by

$$C(x,t') = \int_0^{t'} F(\tau) \frac{\partial A}{\partial t'} (x, t' - \tau) d\tau \qquad A.6$$

where F(t') is the prescribed time dependent surface concentration and A(x,t') is the concentration within the body for the condition that F(t') = 1. The function A(x,t') is obtained from the standard solution to the diffusion equation with time independent surface conditions. It is emphasized that $F(\tau)$ is also transformed according to Eq. (A.5). This is accomplished by finding the inverse $[I^{-1}(t')]$ of Eq. (A.4) and using the physical fact that $T(t) = T(\tau)$ so that

$$T(\tau) = T[I^{-1}(t')]. \qquad A.7$$

We are now in a position to find the mean vacancy concentration ($\bar{c}(t')$) in the lattice for any possible source. The sources we consider are free surfaces, subgrain boundaries and dislocations. The problem of the free surface is analogous to that of diffusion into a slab of thickness L'. The quantity L' is at least four times smaller than the other two dimensions of the crystal so we can neglect the flux from their surfaces. To solve the diffusion equation for the subgrain problem we replace them by spheres of an equivalent radius a, where a is determined from back reflection x-ray Lauegrams. For dislocations, a model consisting of a regular array of dislocations is employed. The array is then replaced by a single dislocation enclosed in a cylinder of outer

radius R and inner radius b. With these three models in mind we will now proceed to the formal solutions.

The problem of the surface source is solved for the following boundary conditions;

$$C = 0 \qquad t = 0 \qquad 0 < x < L'$$
$$C(t) = e^{S^f_{1v}/k} e^{-E^f_{1v}/kT(t)} \qquad t > 0 \qquad x = L' = 0 \qquad \text{A.8}$$

The solution for the concentration profiles is

$$C(x,t') = \frac{2}{\pi\lambda}\sum_{n=1}^{\infty}[(-1)^{n+1}+1]n\left\{\int_0^{t'} e^{n^2\tau/\lambda}\cdot F(\tau)d\tau\right\}\sin\left(\frac{n\pi x}{L'}\right)e^{-n^2t'/\lambda}, \qquad \text{A.9}$$

and the mean vacancy concentration is found by integrating Eq. (A.9) over the volume of the slab which leads to,

$$\bar{C}(t') = \frac{2\pi}{\lambda^2}\sum_{n=1}^{\infty}[1+(-1)^{n+1}]^2\left\{\int_0^{t'} e^{n^2\tau/\lambda}F(\tau)d\tau\right\}e^{-n^2t'/\lambda}, \qquad \text{A.10}$$

where $\lambda = (L'/\pi)^2$.

The problem of subgrain source action employs the following boundary conditions;

$$C=0 \qquad t=0 \qquad 0<\rho<a \qquad \text{A.11}$$
$$C(t) = e^{S^f_{iv}/k} e^{-E^f_{iv}/kT(t)} \qquad t>0 \qquad \rho=a$$

Employing Eq. (A.6) the expression obtained is

$$C(\rho,t') = \frac{2a}{\pi\rho\lambda}\sum_{n=1}^{\infty}(-1)^{n+1}n\left\{\int_0^{t'}F(\tau)e^{n^2\tau/\lambda}d\tau\right\}\sin\left(\frac{n\pi\rho}{a}\right)e^{-t'n^2/\lambda} \qquad \text{A.12}$$

where $\lambda = (a/\pi)^2$. Similarly integrating Eq. (A.12) over the volume of the sphere yields

$$\bar{C}(t')=\frac{6}{\pi^2\lambda}\sum_{n=1}^{\infty}\left[\int_0^{t'}F(\tau)e^{n^2\tau/\lambda}\,d\tau\right]e^{-t'n^2/\lambda} \qquad \text{A.13}$$

Lastly, the problem for the dislocation is solved under the following conditions:

$$\begin{aligned} &C(t)=e^{S^f_{iv}/k}e^{-E^f_{iv}/kT(t)} && t>0 && r=b \\ &(\partial C/\partial r)=0 && \text{all } t && r=R \\ &C=0 && t=0 && b<r\leqq R \end{aligned} \qquad \text{A.14}$$

Once again by applying Duhamel's theorem we obtain,

$$C(r,t')=\pi\sum_{n=1}^{\infty}\alpha_n^2\int_0^{t'}F(\tau)e^{\alpha_n^2\tau}d\tau\left[\frac{J_1^2(R\alpha_n)\left[J_0(b\alpha_n)Y_0(r\alpha_n)-J_0(r\alpha_n)Y_0(b\alpha_n)\right]}{J_0^2(b\alpha_n)-J_1^2(R\alpha_n)}\right]e^{-t'\alpha_n^2} \qquad \text{A.15}$$

and then by integration the mean vacancy concentration is

$$\bar{C}(t')=\frac{2\pi}{R^2-b^2}\sum_{n=1}^{\infty}\left\{\int_0^{t'}F(t)e^{\alpha_n^2\tau}d\tau\right\}\left[\frac{b\alpha_n J_1^2(R\alpha_n)\left[Y_0(b\alpha_n)J_1(b\alpha_n)-J_0(b\alpha_n)Y_1(b\alpha_n)\right]}{J_0^2(b\alpha_n)-J_1^2(R\alpha_n)}\right]e^{-t'\alpha_n^2} \qquad \text{A.16}$$

The α_n are the roots of

$$Y_0(b\alpha_n)J_1(R\alpha_n)-J_0(b\alpha_n)Y_1(R\alpha_n)=0 \qquad \text{A.17}$$

where $F(\tau)$ is as previously defined and $J_n(X)$ and $Y_n(X)$ are Bessel Functions of the first and second kind of order n. The eigenvalues α_n are relatively insensitive to the choice of b and a standard value of 3A is employed, while the values of R are given by $(4N_d)^{-1/2}$ where N_d is the number of dis-

locations cm^{-2}.

The three Eq. (A.10), (A.13) and (A.16) are summed on an IBM 7094 employing the following parameters;

Parameter	Name	Value	Source
S^f_{1v}/k	Vibrational entropy of formation factor for a monovacancy	1.2	Simmons and Balluffi, 1962
E^f_{1v}	Energy of formation of a single vacancy	0.98eV	Bass, 1964 Bass and Flynn, 1965
E^m_{1v}	Energy of migration of a single vacancy	0.85eV	Bass, 1964 Bass and Flynn, 1965 Ytterhus, 1964
	rate constant for upquenching	5.5 sec^{-1}	This experiment
D_{01v}	pre-exponential factor for monovacancy diffusion	0.0358$cm^2 sec^{-1}$	Simmons and Balluffi, 1962 Makin et al, 1957

To show the importance of the present time dependent calculations a comparison is made in Fig. 13 of the solution to Eq. (A.16) for $N_d = 10^7 cm^{-2}$ and $\alpha = 5.5\ sec^{-1}$ (curve III), $\alpha = 10\ sec^{-1}$ (curve II) and $\alpha \longrightarrow \infty$ (I). The final curve (I) is simply the isothermal solution and is found by letting $Dt^{\frac{1}{2}} \longrightarrow Dt$ and $F(\tau) \longrightarrow C_o$. It is readily seen that the upquenching rate is an important parameter in this

problem and emphasizes the need to include time dependent boundary conditions and a temperature dependent monovacancy diffusion coefficient.

APPENDIX B

SOLUTION OF THE DIFFUSION EQUATION FOR COMBINED RADIAL AND AXIAL FLOW FROM THE GRAIN BOUNDARIES AND FREE SURFACE

In Sec. III B we used the results of a diffusion calculation to show that the grain boundary and free surface make a negligible contribution to the experimentally determined generation kinetic curves. This appendix contains an outline of that calculation and a discussion of the model employed.

Metallographic examination of the polycrystalline foils shows that a good mathematical approximation to the grains is a pillbox of height L' and radius A. The diffusion equation is then solved for simultaneous flow from surfaces separated by a distance L' and grain boundaries which are the sides of the pillbox. The general solution for combined radial and axial flow is (Carslaw and Jaeger, 1959),

$$C(z,r,t) = 1 - \psi(z,L',t) \cdot \zeta(r,a,t) \qquad \text{B.1}$$

Where $\psi(z,L',t)$ is the function appropriate to the slab $0 < z <$ L' with unit initial concentration and with surfaces kept at zero concentration. The function $\zeta(r,a,t)$ is the solution to the diffusion equation for an infinite cylinder with unit initial concentration and zero surface concentration. If Eq. (B.1) is integrated over the volume of the cylinder, the mean vacancy concentration as a function of time is

$$f(t) = 1 - \frac{8}{\pi^2} \sum_{n=1}^{\infty} \frac{[1-(-1)^n]^2 \, EXP\left[-D_{iv} t \left(\frac{n^2\pi^2}{L'^2} + \frac{B_n^2}{a^2}\right)\right]}{n^2 B_n^2} \qquad \text{B.2}$$

where $B_n = a \alpha_n$ and the B_n are the zeroes of the Bessel function $[J_o (B_n)]$ of the first kind of order zero.

APPENDIX C

CALCULATION OF THE PIPE DIFFUSION COEFFICIENT (D_p) REQUIRED TO MAINTAIN A GIVEN FLUX (φ) INTO THE LATTICE

In this appendix we show that the generated vacancies are not produced at the specimen surfaces and then piped into the specimen via dislocation short circuiting paths. This is accomplished by demonstrating that an impossibly large pipe diffusion coefficient (D_p) is necessary to supply the total measured values of the vacancy flux into the specimen.

Consider a pipe of radius r_o and length Λ to lie along the z - axis. The pipe is connected to a source of vacancies at either end ($z = 0$ and $z = L$). The source may be a surface, grain boundary or sub-boundary wall. We then apply the following boundary conditions

$$C = C_o \qquad \text{at} \quad z = 0 = \Lambda \qquad \text{C.1}$$

$$\frac{\partial c}{\partial z} = 0 \qquad \text{at} \quad z = \Lambda/2 \qquad \text{C.2}$$

$$C = C_{o/n} \qquad \text{at} \quad z = \Lambda/2 \qquad \text{C.3}$$

The boundary condition (C.3) fixes the deviation from equilibrium where n is any positive integer greater than 1. For example, $n = 2$ implies that at $z = \frac{\Lambda}{2}$ the vacancy concentration is one-half its equilibrium value C_o.

Consider an element of pipe of length dz and radius r_o. Next we use the equation of continuity to find the steady state vacancy distribution in the dislocation core along the z-axis under the condition that φ vacancies cm^2

sec^{-1} are leaking out of the element dz of pipe in the r-direction. The assumption of a steady state distribution in the core is reasonable in view of our general requirement that the cores act as essentially constant vacancy sources, maintained near the equilibrium concentration and the fact that extremely fast pipe diffusion diffusivities are required. Therefore, the equation of continuity is

$$\pi \mathcal{R}_o^2 dz \frac{\partial c}{\partial t} = \left\{ -\pi \mathcal{R}_o^2 D_p - \pi \mathcal{R}_o^2 D_p \left[-\frac{\partial c}{\partial z} - \frac{\partial}{\partial z}\left(\frac{\partial c}{\partial z}\right) dz \right] - 2\pi \mathcal{R}_o \phi dz \right\} \qquad \text{C.4}$$

which reduces to

$$D_p \frac{\partial^2 c}{\partial z^2} = \frac{2\phi}{\mathcal{R}_o} \qquad \text{C.5}$$

in the steady state.

Integrating and using boundary conditions (C.1) and (C.2) yields the steady state distribution in terms of D_p, z and ϕ.

$$C(z) = \frac{\phi}{D_p \mathcal{R}_o} z^2 - \frac{\phi \Lambda}{D_p \mathcal{R}_o} z + C_o \qquad \text{C.6}$$

Now by applying Eq. (C.3) we obtain the pipe diffusion coefficient (D_p) in terms of measureable parameters,

$$D_p = \frac{n \quad \phi \quad \Lambda^2}{4(n-1) \; C_o \quad o} \qquad \text{C.7}$$

The vacancy flux ϕ is proportional to the slope of the plot of f(t) versus t(sec) (See Fig. 5 and 6), and is given by the expression,

$$\phi = \frac{C_o}{2\pi \mathcal{H}_o N_d} \left(\frac{df}{dt}\right) \qquad \text{C.8}$$

where N_d (cm cm^{-3}) is the dislocation density and C_o the equilibrium vacancy concentration. Therefore the final expression for the required D_p is given by,

$$D_p = \frac{n\Lambda^2}{(n-1)8\pi \mathcal{H}_o^2 N_d} \left(\frac{df}{dt}\right) \qquad \text{C.9}$$

Evaluating Eq. (C.9) at 878°C for Λ = 0.051 cm, n = 2, $\mathcal{H}_o$ = 3A and $N_d = 3.10^7$ cm cm^{-3} yields the enormous D_p value of $4 \cdot 10^5$ $cm^2 sec^{-1}$ required to support the measured value of (df/dt).

This unreasonably large diffusion coefficient yields the following two physically improbable results;

1) For a value of $(E_{1v}^m)_p$ equal to 0.09eV** the required Debye frequency of an atom in the dislocation is the impossibly large value of about $4 \cdot 10^{20} sec^{-1}$.

2) Conversely if we assume a more reasonable Delye frequency of about 10^{13} sec^{-1} then $(E_{1v}^m)_p$ is an impossible - 1.87eV.

In view of these impossible requirements we conclude that the vacancies produced internally and are not simply piped into the lattice from the surface via dislocation short circuits.

**This is the migration energy of a single vacancy in the pipe calculated by using Turnbull and Hoffman's (1954) result that $Q_p \sim 0.45 Q_1$, where Q_p is the activation energy for pipe diffusion and Q_1 is the activation energy for lattice diffusion.

APPENDIX D

VACANCY DIFFUSION LIMITED CLIMB

1. Solution of the Diffusion Equation

Under the assumptions given in Sec. IV A we solve the axially symmetric diffusion equation

$$\frac{\partial C}{\partial t} = D_{lv} \frac{1}{r} \frac{\partial}{\partial r} \left(r \frac{\partial C}{\partial r} \right), \qquad \text{D.1}$$

with the following boundary conditions

$$C = C_0 \qquad r = b \qquad \text{all } t \qquad \text{D.2}$$

$$C = 0 \qquad b < r \leqq R \qquad t = 0 \qquad \text{D.3}$$

$$\frac{\partial C}{\partial r} = 0 \qquad r = R \qquad \text{all } t \qquad \text{D.4}$$

where C_o is the equilibrium concentration at temperature ($\bar{T}_f$). The boundary condition (D.4) is a result of requiring that C(r,t) have the symmetry of the lattice (Ham 1958, 1959). Carslaw and Jaeger (1959) have solved the diffusion equation for a hollow cylinder with very general boundary conditions. Restricting their results to our boundary conditions gives the solution,

$$C(r,t) = 1 - \pi \sum_{n=1}^{\infty} \frac{J_1^2(R\alpha_n)\left[J_0(b\alpha_n) Y_0(r\alpha_n) - J_0(r\alpha_n) Y_0(b\alpha_n) \right] e^{-Dt\alpha_n^2}}{\left[J_0^2(b\alpha_n) - J_1^2(R\alpha_n) \right]} \qquad \text{D.5}$$

where the α_n are the roots of the equation

$$Y_0(b\alpha_n) J_1(R\alpha_n) - J_0(b\alpha_n) Y_1(R\alpha_n) = 0 \qquad \text{D.6}$$

and the J_n and Y_n are as previously defined. The mean vacancy fraction (f) is found by integrating C(r,t) over the

volume of the cylinder which yields,

$$f(t) = 1 - \frac{2\pi}{R^2 - b^2} \sum_{n=1}^{\infty} \frac{b\alpha_n}{\alpha_n^2} \frac{J_1^2(R\alpha_n)\left[Y_0(b\alpha_n)J_1(b\alpha_n) - J_0(b\alpha_n)Y_1(b\alpha_n)\right]}{\left[J_0^2(b\alpha_n) - J_1^2(R\alpha_n)\right]} e^{-Dt\alpha_n^2} \qquad (D.6)$$

Using the Wronksian relation,

$$J_0(b\alpha_n)Y_0'(b\alpha_n) - Y_0(b\alpha_n)J_0'(b\alpha_n) = 2/\pi b\alpha_n \qquad (D.7)$$

(D.6) reduces to

$$f(t) = 1 - \frac{4}{R^2 - b^2} \sum_{n=1}^{\infty} \frac{J_1^2(R\alpha_n)\exp(-Dt\alpha_n^2)}{\alpha_n^2\left[J_0^2(b\alpha_n) - J_1^2(R\alpha_n)\right]} \qquad D.8$$

The analyses of Ham (1958) on diffusion limited climb precipitation make use of the fact that the largest fraction of the precipitate decays according to the first term in the eigen function expansion and only a small fraction decays according to the higher order terms. In equation (D.8) the fraction of the total vacancies contributed by the nth term is given by

$$\frac{4}{(R^2 - b^2)\alpha_n^2} \frac{J_1^2(R\alpha_n)}{\left[J_0^2(b\alpha_n) - J_1^2(R\alpha_n)\right]} \qquad D.9$$

which yields a value of 0.996 for the lowest component (α_1) with $N_d = 10^7$ cm cm^{-3} and $b = 3 \cdot 10^{-8}$cm. We may therefore safely replace Eq. (D.8) by

$$f \cong 1 - \exp(-\alpha_1^2 Dt) \qquad D.10$$

Next, we define the parameter τ as

$$\frac{1}{\tau} = D_{1v}\alpha_1^2 = 4(R\alpha_1)^2 N_d D_{1v} = \xi N_d D_{1v} \qquad D.11$$

So Eq. (D.10) takes the form

$$f = 1-e^{-t/\tau} = 1-e^{-\xi N_d D_{1v} t} \qquad D.12$$

which is the equation used in Sec. IV A.

2. The Elastic and Electronic Vacancy-Dislocation Interactions

In solving the diffusion equation on (D.1) we have neglected two elastic and one electronic interaction. The two elastic interactions (e.g. see Cottrell, 1953, Bullough and Newman, 1962) have their origins in: (1) A size difference between the vacancy and matrix atoms (E_1).; (2) An interaction due to the vacancy acting as an inclusion with an elastic modulus different from that of the host crystal (E_2). The electronic vacancy-dislocation interaction (Flynn, 1962) is an oscillatory long range interaction modified by an $r^{-5/2}$ dependence. It is the aim of this section to show that the present diffusion problem may be treated by neglecting all the interactions and simply using an "effective capture (emission) radius."

First it is important to determine the magnitude of the interactions. For the elastic interactions E_1 and E_2 the magnitudes are about $-10^{-1}\mu$Ve and $-6.7\cdot10^{7}\mu$V at a distance of 10 Burgers' vectors from the an edge dislocation. Here, μ is the shear modulus, V the volume of a vacancy and e

the radial strain due to the relaxation around a vacancy. Using Simmons and Balluffi's (1962) value of one-half an atomic volume for the volume of a vacancy we find the ratio of E_1/E_2 is 27, so the dominant elastic vacancy-dislocation interaction in gold is the size difference effect (E_1). The short range character of the electronic interaction varies as $r^{-5/2}$ while E_1 has an r^{-1} dependence. Therefore, E_1 is the dominating interaction and we shall focus our attention on it.

Ham (1959) in an elegant paper on "Stress-Assisted Precipitation on Dislocations" obtained an exact solution to the steady-state diffusion equation for the precipitation of solute atoms, on an edge dislocation, in the presence of the elastic interaction (E_1). By comparing this solution to the simple steady-state solution in the absence of an interaction ($E_1 = 0$) he is able to define an "effective capture (emission) radius" for the interaction E_1. This is given by

$$R = (A\, e^{\gamma}/kT)/4 \qquad \text{D.13}$$

where A is a factor made up of elastic constants (Cottrell, 1953) and γ is Euler's constant. He justifies the use of R by solving the time-dependent diffusion equation for the interaction E_1 numerically and comparing it to the analytical time-dependent solution in the absence of a potential gradient ($E_1 = 0$), employing R as the radius of the dislocation core. His results indicate that within 10% (at the worst) the solutions are identical. Using the room temperature elastic

constants of gold we find that R is 6.7A at 653°C and 5.4A at 878°C. Since the eigenvalue α_1 has a logarthmic dependence* on the ratio R/b we conclude that our use of a constant 3A core radius is therefore justified.

3. Effect of the Dislocation Climb Motion

In a forthcoming paper Balluffi and Seidman (1965) consider a regular array of dislocations and calculate the effect of the dislocation motion on the vacancy generation rate. (It is noted that in all of the previous calculations the sources have been assumed to remain stationary and, therefore, any possible effects due to the climb motion are neglected.) They show that the general effect of the climb motion is to speed up the generation rate (relative to assumed stationary sources) and that the size of the effect is determined by the magnitude of the parameter $vR/2D_{1v}$, where v is the climb velocity. For the case $vR/2D_{1v} << 1$ the climb velocity is identical to that found by assuming stationary dislocations. For the extreme case $vR/2D_{1v} >> 1$, the ratio of the climb velocities is

$$\frac{v_2(t)}{v_1(t)} = \frac{\ln(R/b)}{\ln(4D_{1v}/bv_2)} \qquad D.14$$

where v_1 is the velocity of a dislocation in an array con-

---

*The lowest eigenvalue (α_1) is given approximately by $\alpha_1^2 \simeq \frac{2}{R^2}\left[\ln(R/b) - 3/5\right]^{-1}$. See Ham (1959) for further details.

sidered to be stationary and v_2 is the climb velocity when the effect of climb is taken into account.

It is of interest to calculate the magnitude of $vR/2D_{1v}$ for the present experiments to see if the climb motion affects the generation kinetics. The climb velocity is proportional to the slope (df/dt) of the generation curve, since df/dt is simply the climb rate (χ). The results for this experiment, using the value of (df/dt) at the half-time, are

$vR/2D_{1v}$*	T^oC
$3.9 \cdot 10^{-2}$	653
$5.7 \cdot 10^{-2}$	875

Therefore we conclude that the stationary approximation is a satisfactory one for the present experiment.

---

*These are calculated for $N_d = 3 \cdot 10^7$ cm cm^{-3} and a total climb distance (x_c) given by $4N_{1v}^d/3a_o \sqrt{2}\, N_d$. Where N_{1v} is the equilibrium vacancy concentration.

APPENDIX E

CALCULATION OF THE JOG ENERGY BASED ON A HOMOGENEOUS CLIMB MODEL

The basic equations derived by Thomson and Balluffi (1962) for the case of negative climb in the presence of a subsaturation of vacancies ($S < 0$) are given in the following table

αL	χ	L
$\alpha L < 3$	$B\phi_0 S$	L_0
$\alpha L > 3$	$2B\phi_0 S/\alpha L$	$L_0\left[1+S\left(1-\frac{2}{\alpha L}\right)\right]^{(\Lambda'-1)/2}$

The quantity χ is the climb rate (sec^{-1}), B a geometric factor, ϕ_0 the flux of vacancies from the dislocation, the convergence length of a well formed jog pair, and all the other parameters are as defined previously. The parameter α is approximately given by $\exp(-Q_1/4kT)$ where Q_1 is the activation energy for self-diffusion.

An estimate of the jog energy under the assumptions of vacancy DLDC and homogeneous climb can be obtained from the simple criterion $\alpha L_0 < 3$.* Therefore, $\mathcal{E}_j$ is

$$\mathcal{E}_j < Q_e/4 + kT\ln 3 \qquad \text{E.1}$$

This result yields about 0.6eV as previously discussed.

---

*L_0 is given by the standard Boltzmann factor, $\exp(\mathcal{E}_j/kT)$.

The transition point from DLDC to PLDC occurs about when $\alpha L = 3$ in the relation

$$\alpha L = \alpha L_0 \left[1 + S_c \left(1 - \frac{2}{\alpha L}\right)\right]^{(\Lambda'-1)/2}, \qquad \text{E.2}$$

where S_c is the critical subsaturation at which the transition occurs. Solving for S_c, one obtains

$$S_c = 3\left\{9^{\frac{1}{\Lambda'-1}} \exp\left[\frac{-2(\varepsilon_j - \Omega_1/4)}{kT(\Lambda'-1)}\right] - 1\right\}. \qquad \text{E.3}$$

Thus, the value of S_c is a function of Λ' and ε_j at any fixed temperature. For a fixed jog energy the value of S_c decreases (i.e. becomes more negative) as Λ' increases.

For a detailed discussion of the problem of the kinetics of homogeneous climb and the limitations of the above formulae the reader is referred to the Thomson-Balluffi papers.

APPENDIX F

COMMENTS ON THE DISTRIBUTION OF DISLOCATION DENSITIES THROUGHOUT THE SPECIMENS

In Sec. IV A we stated that the measured dislocation density distributions are non-Poisson in character and hence the free dislocations are non-randomly distributed with respect to a Poisson distribution. In this appendix a short discussion of the statistics involved is presented to support the above statement.

The total area that may be sampled in a given polycrystalline specimen is about 0.45 cm^2, while each micrograph* samples only 24.4 μ^2. Therefore below a dislocation density of about $8 \cdot 10^6$ cm cm^{-3} (i.e., one dislocation per micrograph) the sampling problem becomes very difficult. Each distribution is based on 150 to 300 micrographs taken at random**. Hence the total fraction of area sampled is about $8.2 \cdot 10^{-5}$ for each specimen.

The data are plotted in the form of distributions normalized to unity, i.e., in each case the fraction (F(n) of the total number of plates with a given number (n) of dislocations is plotted against the number (n) of dislocations. The variance (average number of dislocations per micrograph) is

---

*This is at a standard magnification of 15,000x.

**More exactly, the micrographs are taken at random in regions away from the thin edges of the foil.

determined, and this variance is then used to calculate the expected fraction f(n) of plates with a given n on the assumption that the distribution of dislocations obeys a Poisson distribution. The goodness of fit is then checked using the standard χ^2 test (e.g., Parratt, 1961). For example, the distribution for the specimens pulsed to 878°C (See Fig. 7) has a probability of less than 10^{-3} of fitting a Poisson distribution on the basis of the χ^2 test. The main reason for the poorness of the fit is that the measured distribution has a higher fraction of plates with low n values than the calculated Poisson distribution. This result is hardly surprising since we would expect the dislocations in highly deformed and recrystallized metals to be nonrandomly distributed.

APPENDIX G

THE INTERNAL STRESS DISTRIBUTION IN A FOIL OF RECTANGULAR CROSS-SECTION CAUSED BY THE PASSAGE OF LARGE CURRENTS

The passage of a heavy current through a conductor results in an internal stress distribution. Northrup (1907) has calculated the stress distribution in a wire of circular cross-section. For that case the pressure is purely radial assuming that the wire has isotropic elastic properties. In this appendix we derive equations for the internal stress distribution in a foil of rectangular cross-section and obtain an equation for the electric current required to cause slip.

Consider a foil of length L, thickness 2t, and width 2w to lie along the z-axis. The width 2w is 10t for the cross-section of interest. Make a cut through the foil at the $z = 0$ plane and align the x and y axes so that the $x = 0$ plane cuts the cross-section at t and the $y = 0$ plane cuts it at w. We will now calculate the internal stress σ_{xx}, where σ_{xx} is the stress in the x direction on the $x = x$ plane. The current density is assumed to be constant throughout the cross-section. Therefore the current i at x is

$$i = \frac{I}{2}\left(\frac{x}{t}\right). \qquad \text{G.1}$$

Next we employ the Circuital Law to obtain the magnetic field B_y, since the force in the x-direction is $-ev\,B_y$. The Circuital Law is

$$\oint \vec{B}\cdot d\vec{\ell} = 4\pi\mu\mu_0 i \qquad \text{G.2}$$

Therefore, B_y is <u>approximately</u> given by

$$B_y \simeq \pi \mu \mu_o I (x/t) / (2w+x) \qquad \text{G.3}$$

Now, consider an element of foil of thickness dx at a distance x from the x = 0 plane. The element of current dI passing through dx is

$$dI = \frac{dx}{2} \frac{I}{t} \qquad \text{G.4}$$

and the force per unit length on this element is $B_y dI$. Thus, the increment of stress ($d\sigma_{xx}$) is $B_y dI/2w$. Integrating to find the total stress as a function of x, we obtain

$$\sigma_{xx} \simeq \frac{\pi \mu \mu_o}{4wt^2} I^2 [t - x + 2w \ln(2w+x)/(2w+t)] \qquad \text{G.5}$$

The maximum stress occurs on the x = 0 plane and is given by

$$(\sigma_{xx})_{MAX} \simeq \frac{\pi \mu \mu_o}{4wt^2} I^2 [t + 2w \ln(2w)/(2w+t)] \qquad \text{G.6}$$

which reduces to

$$(\sigma_{xx})_{MAX} \simeq \frac{\pi \mu \mu_o}{20t^2} [1 + 10 \ln(10/11)] \qquad \text{G.7}$$

upon substitution of $2w = 10t$.

As a result of the compressive stress in the x directions there will tend to be lateral expansions in the z and y directions given by

$$\epsilon_{yy} = \epsilon_{zz} = -\nu \epsilon_{xx} = -\frac{\nu \sigma_{xx}}{E} \qquad \text{G.8}$$

where ν is Poisson's ratio. However, to keep the planes $y = \pm w$ and $z = \pm L/2$ planar, a stress (σ) of magnitude

$$\sigma = \frac{\sigma_{yy}}{2} = \frac{\sigma_{zz}}{2} = -\frac{\nu\sigma_{xx}}{2} \qquad \text{G.9}$$

is developed. For $\nu = 0.42$ this stress is $-0.21\ \sigma_{xx}$. Thus the internal stress distribution is far from being hydrostatic and deformation can occur.

Since deformation will occur where the shear stress is a maximum we must maximize the resolved shear (τ) in a plane making an angle Θ with the x-axis. The quantity τ is given by

$$\tau = \sigma_{xx} \sin\Theta\cos\Theta \qquad \text{G.10}$$

which is a maximum ($\frac{d\tau}{d\Theta} = 0$) for $\Theta = \pi/4$. Therefore $\sigma_{xx} = 2\tau$. We now simply solve for I and obtain an expression for the critical current (I_c) to cause slip; therefore,

$$I_c \simeq \left[\frac{40t^2\tau}{\pi\mu\mu_0}\right]^{1/2} \qquad \text{G.11}$$

This result is probably an overestimate of I_c as we have no way to take into account any local inhomogeneities, which would tend to concentrate the magnetic field and therefore increase the stresses.

BIBLIOGRAPHY

Bailey, J. E., and Hirsch, P. B., 1960, Phil Mag., 5, 485.

Balluffi, R. W., Koehler, J. S. and Simmons, R. O., 1963, in Recovery and Recrystallization (Interscience Publishers, New York), P. 1.

Balluffi, R. W., and Seidman, D. N., 1965, to be published.

Bardeen, J. and Herring, C., 1952, in Imperfections in Nearly Perfect Crystals (John Wiley and Sons, New York), p. 261.

Barnes, R. S., 1960, Phil. Mag., 5, 635.

Basinski, Z. S., 1964, private communication.

Basinski, Z. S., Dugdale, J. S., and Howie, A., 1963, Phil. Mag., 8, 1992.

Bass, J., 1964, Ph.D. Thesis, University of Illinois.

Bass, J., and Flynn, C. P., 1965, to appear in Phil. Mag.

Bullough, R., and Newman, R. C., 1962, Phil. Mag., 7, 529.

Carslaw, H. S., and Jaeger, J. C., 1959, in Conduction of Heat in Solids (Oxford University Press, 2nd Edition), pp. 30, 99, 199, 233, 332.

Cottrell, A. H., 1953, in Dislocations and Plastic Flow in Crystals (Oxford University Press), pp. 57, 74.

Escaig, B., 1963, Acta Met. 11, 595.

Flynn, C. P., 1962, Phys. Rev., 125, 881.

Flynn, C. P., 1964, Phys. Rev., A 133, 857.

Frank, F. C., 1957, Proc. Phys. Soc. (London), B70, 1022.

Friedel, J., 1964, in Dislocations (Pergamon Press), Chap. 5.

Ham, F. S., 1958, J. Phys. Chem. Solids, 6, 335.

Ham, F. S., 1959, J. Appl. Phys., 30, 915.

Ham, R. K., 1961, Phil. Mag., 6, 1183.

Ham, R. K. and Sharpe, N. G., 1961, Phil. Mag., 6, 1193.

Hildebrand, F. B., 1964, in Advanced Calculus for Applications (Prentice-Hall, Inc.), p. 451.

Hirsch, P. B., 1962, Phil. Mag. 7, 67.

Jackson, J. J., 1960, Ph.D. Thesis, University of Illinois.

Koehler, J. S., 1964, Private Communication.

Koehler, J. S., and Lund, C. A., 1964, in Proceedings of the International Conference on Lattice Defects in Quenched Metals, in the press.

Lothe, J., 1960, J. Appl. Phys. 31, 1086.

Lund, C. A., 1964, Ph.D. Thesis, University of Illinois.

Makin, S. M., Rowe, A. H., and LeClaire, A. D., 1957, Proc. Phys. Soc. (London), B70, 545.

Meechan, C. J. and R. R. Eggleston, 1954, Acta. Met., 2, 680.

Mott, N. F., 1951, Proc. Phys. Soc. (London) B64, 729.

Northrup, E. F., 1907, Phys. Rev. 20, 474.

Parratt, L. G., 1961, in Probability and Experimental Errors in Science (John Wiley and Sons, Inc. New York), p. 195.

Schulz, L. G., 1954, J. of Met., 200, 1082.

Seeger, A., 1955, in Report of the Conference on Defects in Crystalline Solids (The Physical Society), p. 396.

Seidman, D. N. and Balluffi, R. W., 1964, Phil. Mag., 10, 1067.

Siegel, R. W., 1965, Ph.D. Thesis, University of Illinois.

Simmons, R. O. and Balluffi, R. W., 1962, Phys. Rev., 125, 862.

Smith, C. S., and Guttman, L., 1953, J. Metals, 5, 85.

Thomson, R. M., and Balluffi, R. W., 1962, J. Appl. Phys, 33, 803; 1962, 33, 817.

Thornton, P. R. and Hirsch, P. B., 1958, Phil. Mag., 3, 738.

Turnbull, D., and Hoffman, R. E., 1954, Acta. Met., 419.

Weertman, J., 1955, J. Appl. Phys., 26, 1213.

Weertman, J., 1957, J. Appl. Phys., 28, 362.

Young, F. W. and Savage, J. R., 1964, J. Appl. Phys., 35, 1917.

Ytterhus, J. A., 1964, Ph.D. Thesis, University of Illinois.

Ytterhus, J. A., and Balluffi, R. W., 1965, to be published in Phil. Mag.

VITA

David N. Seidman was born in Brooklyn, New York on July 5, 1938. He received his elementary school education at the Public Schools in Jackson Heights, New York and was graduated from the Brooklyn Technical High School in 1956. His Bachelors and Masters degrees were received from New York University in 1960 and 1962 respectively. While at New York University he was elected to membership in Tau Beta Pi and Alpha Sigma Mu and was the holder of a University scholarship. Since February 1962 he has been a Research Assistant in the Department of Mining, Metallurgy and Petroleum Engineering at the University of Illinois. He is a member of the A.I.M.E. and his publications include:

1. D. Seidman, I. Cadoff, K. Komarek and E. Miller, "Note on the Pb-Se Diagram," Trans. A.I.M.E. 221, 1269 (1961).
2. D. N. Seidman and R. W. Balluffi, "Vacancy Annealing in Quenched and Deformed Gold: Tetrahedron Formation at Vacancy Type Dislocation Debris Along $\langle 110 \rangle$ Directions," Phil. Mag. 10, 1067, (1964).
3. D. N. Seidman, "The Stoichiometry of Lead Selenide and the Partial Lead (0-76 at.%) - Selenium Phase Diagram (to be submitted to the Trans A.I.M.E.).